Characterizing Tropical Cirrus Life Cycle, Evolution, and Interaction with Upper-Tropospheric Water Vapor Using Lagrangian Trajectory Analysis of Satellite Observations

Zhengzhao Luo

Cooperative Institute for Research in the Atmosphere, Colorado State University, Fort Collins, Colorado

William B. Rossow

NASA Goddard Institute for Space Studies, New York, New York

ABSTRACT

Tropical cirrus evolution and its relation to upper-tropospheric water vapor (UTWV) are examined in the paper by analyzing satellite-derived cloud data, UTWV data from infrared and microwave measurements, and the NCEP–NCAR reanalysis wind field. Building upon the existing International Satellite Cloud Climatology Project (ISCCP) data and the Television and Infrared Observation Satellite (TIROS) Operational Vertical Sounder (TOVS) product, a global (except polar region), 6-hourly cirrus dataset is developed from two infrared radiance measurements at 11 and 12 μm. The UTWV is obtained in both clear and cloudy locations by developing a combined satellite infrared and microwave-based retrieval. The analysis in this study is conducted in a Lagrangian framework. The Lagrangian trajectory analysis shows that the decay of deep convection is immediately followed by the growth of cirrostratus and cirrus, and then the decay of cirrostratus is followed by the continued growth of cirrus. Cirrus properties continuously evolve along the trajectories as they gradually thin out and move to the lower levels. Typical tropical cirrus systems last for 19–30 $\pm$ 16 h. This is much longer than cirrus particle lifetimes, suggesting that other processes (e.g., large-scale lifting) replenish the particles to maintain tropical cirrus. Consequently, tropical cirrus can advect over large distances, about 600–1000 km, during their lifetimes. For almost all current GCMs, this distance spans more than one grid box, requiring that the water vapor and cloud water budgets include an advection term. Based on their relationship to convective systems, detrainment cirrus are distinguished from in situ cirrus. It is found that more than half of the tropical cirrus are formed in situ well away from convection. The interaction between cirrus and UTWV is explored by comparing the evolution of the UTWV along composite clear trajectories and trajectories with cirrus. Cirrus are found to be associated with a moister upper troposphere and a slower rate of decrease of UTWV. Moreover, the elevated UTWV has a longer duration than cirrus. The amount of water in cirrus is too small for evaporation of cirrus ice particles to moisten the upper troposphere significantly (but cirrus may be an important water vapor sink). Rather, it is likely that the same transient motions that produce the cirrus also transport water vapor upward to maintain a larger UTWV.

1. Introduction

Tropical cirrus have been difficult to study because of their great altitude and the extreme conditions in which they occur. Some studies suggest that the response of tropical cirrus to external climate forcing might have a controlling effect on global climate sensitivity [Cirrus Regional Study of Tropical Anvils and Cirrus Layers (CRYSTAL) Research Plan 2000]. Usually, tropical cirrus are thought to originate in outflow from deep convective systems, producing a wide range of high-level clouds from thick anvils to thin cirrus that are sometimes all called cirrus, but other dynamic processes, such as the mesoscale circulations of larger storm systems, large-scale lifting or gravity waves, can also produce cirrus. Beyond this, very little is known, at present, about the distribution of tropical cirrus, their variability, and formation-decay processes.

Tropical cirrus have been studied in a number of field campaigns. The Tropical Ocean Global Atmosphere Coupled Ocean–Atmosphere Response Experiment (TOGA COARE), although focusing mostly on sea–air interaction and deep convective clouds, obtained some observations that have been used to study cirrus anvils in the tropical west Pacific (Ye 2000). The Central Equatorial Pacific Experiment (CEPEX) also made measurements of the microphysical properties of tropical cirrus anvils (McFarquhar and Heymsfield 1996), which clar-

Corresponding author address: Dr. William B. Rossow, NASA Goddard Institute for Space Studies, 2880 Broadway, New York, NY 10025.
E-mail: wrossow@giss.nasa.gov

ified the association between the cirrus microphysical properties and their relative high albedo (Heymsfield and McFarquhar 1996). A recent scientific program more dedicated to tropical cirrus [Cirrus Regional Study of Tropical Anvils and Cirrus Layers–Florida Area Cirrus Experiment (CRYSTAL–FACE)] was carried out in July 2002 to investigate tropical cirrus cloud physical properties and formation processes.

These field programs enhance our understanding of some aspects of tropical cirrus. CRYSTAL-FACE, for example, measured cirrus anvil properties through as much of the cloud life cycle as possible to advance our knowledge of the evolution of cirrus anvils. However, these fields campaigns are all very limited in space and time, making it difficult to study larger-scale cirrus processes and their seasonal/geographical variations and preventing us from developing and generalizing an understanding of how cirrus form, evolve, and dissipate. In contrast, satellite observations have provided a global overview of cloud systems at the mesoscale to the synoptic scale for more than three decades. To understand cirrus evolution processes globally over a long period of time, we still need to analyze these satellite data.

The last three decades have witnessed numerous specialized cirrus retrieval algorithms from satellite measurements, where we use the word cirrus to refer exclusively to the optically thinner (transparent to infrared radiation) high-altitude clouds (e.g., Chahine 1974; Szejwach 1982; Inoue 1985; Liou et al. 1990; Wylie et al. 1994; Stubenrauch et al. 1999a). Nevertheless, very few of these analysis methods have been applied to satellite data to produce globally uniform, long-term cirrus datasets; the notable exceptions are Wylie et al. (1994), Wylie and Menzel (1999), and Stubenrauch et al. (1999b). The International Satellite Cloud Climatology Project (ISCCP), since its establishment in 1982, has produced an 18-yr-long (so far), 3-hourly–30-km cloud climatology (Schiffer and Rossow 1983; Rossow and Schiffer 1991, 1999). Sensitivity to cirrus has been increased and biases in cirrus optical thickness are reduced in the second version (D series) of the ISCCP cloud product (Rossow and Schiffer 1999). ISCCP retrieves cloud properties from infrared (≈ 11 μm) and visible (≈ 0.6 μm) radiances measured by the imaging instruments on all of the operational weather satellites, so specific cirrus information is available only during daytime. Several studies have quantified the successes and limitations of the ISCCP cirrus representation (Liao et al. 1995a,b; Jin et al. 1996; Jin and Rossow 1997; Stubenrauch et al. 1999a; Luo et al. 2002). In our study of cirrus variability and evolution, we develop a refined cirrus dataset derived from only infrared observations by building upon the existing ISCCP DX data and TIROS-N Operational Vertical Sounder (TOVS) products. This cirrus dataset provides continuous coverage throughout each day by using two radiances from the IR window spectrum at roughly 11 and 12 μm. Comparison with the ISCCP cirrus products will be shown.

We make use of the cirrus dataset to examine the variability of tropical cirrus and to study their life cycle and evolution. Specifically, the following questions are explored: 1) What is the relative importance of deep convection and other dynamical processes in producing cirrus? 2) How long do tropical cirrus last and how do cirrus properties evolve during their life cycle? It is not clear over the whole Tropics how many cirrus are derived from convection and how many are produced in situ by other dynamical processes. Heymsfield and Donner (1990) estimated the frequency of observing cumulonimbus and cirrus simultaneously, but this does not provide an unambiguous answer because they did not follow the life cycle of the cirrus anvils and could not determine where to draw a line between cirrus formed out of convection and cirrus formed elsewhere by other processes. Recently, Pfister et al. (2001) and Massie et al. (2002) studied the different origins for tropical tropopause subvisible cirrus using aircraft and satellite occultation measurements coupled with a back-trajectory method. Massie et al. (2002) found that deep convection was encountered only 49% of the time along the 5-day back-trajectories for the regions 20°S–20°N and 60°E–180°. A common assumption, when discussing cirrus feedback, is that all tropical cirrus are derived from or closely linked to convective systems, technically reducing the cirrus feedback to a "convection–SST" relationship (e.g., Ramanathan and Collins 1991; Chou and Neelin 1999; Lindzen et al. 2001). However, as shown in this study, this is not the case; more than half of tropical cirrus are only loosely, if at all, connected to convection and thus tend to have dynamics of their own. Deep convection can produce a wide range of high-level clouds evolving from thick anvils to cirrus. Cirrus produced in situ may have their own way of forming, evolving, and decaying. However, there has been no global survey of tropical cirrus life cycles and no study of cirrus lifetime duration, let alone the evolution of cirrus properties. To characterize cirrus life cycle and evolution processes, we developed a Lagrangian trajectory method that tracks tropical cirrus systems by following upper-tropospheric air masses using winds from the National Centers for Environmental Prediction–National Center for Atmospheric Research (NCEP–NCAR) reanalysis.

We complement the cloud measurements with determinations of upper-tropospheric water vapor (UTWV) to examine its interaction with cirrus. The key to this study is the development of a technique for determining UTWV in the presence of cirrus by a combined analysis of satellite infrared and microwave radiances. This allows us for the first time to follow the evolution of both UTWV and cirrus. The mesoscale convective systems transport a lot of water upward and thus serve as a water vapor source for the vast tropical (30°S–30°N[1]) upper

---

[1] We follow this definition of the Tropics throughout this paper; it actually includes both the Tropics and subtropics.

troposphere, but the area coverage of these convective systems is very small: about 0.03 of the $\pm 30°$ zone according to the ISCCP. The rest of the tropical upper troposphere is either covered with cirrus (0.14), cirrostratus (0.05) according to ISCCP, or no clouds in the upper troposphere (here taken to be about the 440 mb or 7-km level). The thinnest cirrus that ISCCP misses but other satellite instruments (e.g., solar occultation measurements) detect can cover another 0.05–0.10 of the Tropics (Liao et al. 1995a; Jin et al. 1996; Stubenrauch et al. 1999a). In addition, subvisual tropopause cirrus (optical thickness < 0.03) not discussed in this study cover approximately another 0.15^2 of the Tropics (Wang et al. 1996). How cirrus interact with UTWV is still an open question and invites many hypotheses and speculations. Sun and Lindzen (1993) suggest that the upper-tropospheric hydrometeors are the source for moistening the dry regions of the Tropics, while many other researchers find that cirrus beyond the vicinity of deep convective systems play only a minor role in affecting the UTWV distribution (Salathe and Hartmann 1997; Pierrehumbert and Roca 1998; Dessler and Sherwood 2000). However, lack of collocated cirrus and UTWV datasets makes it difficult to verify the previous studies. For example, the conclusion that cirrus may only be a minor player outside the convective regions is based on the indirect evidence that the UTWV distribution can be simulated reasonably well without considering cirrus interaction. By analyzing the collocated, satellite-derived cirrus and UTWV datasets, we explore the following questions: 1) What is the relationship between cirrus and UTWV? 2) How is UTWV maintained as air makes its way from convective regions to the subtropical dry regions? 3) What role do cirrus play in affecting the UTWV distribution?

The paper is organized as follows. Cirrus and UTWV datasets used in this study are described in section 2, where cirrus from the split-window method and the ISCCP are briefly compared. Section 3 describes the Lagrangian trajectory method and how it is implemented in this study. In section 4, the trajectory analysis is applied to the cirrus dataset to characterize the evolution and life cycle of tropical cirrus. Section 5 estimates the relative abundance of different cirrus-generating mechanisms and their geographical distribution. Section 6 examines the relationship between cirrus and the UTWV, and section 7 discusses the maintenance of UTWV along Lagrangian forward trajectories using a simple, conceptual model. Finally, section 8 summarizes the results and examines them for their implications for cirrus modeling and for cirrus–UTWV feedback on climate changes.

---

^{2} Wang et al. (1996) found that the frequency of occurrence for subvisual cirrus is 0.45, which is equivalent to around 0.15 in terms of cloud cover.

2. Cirrus and upper-tropospheric water vapor datasets

a. The split-window cirrus data

The main reason for using the split-window data is to augment the ISCCP analysis of cirrus during night, when the visible channel becomes unavailable for retrieving cloud optical thickness. The use of 11- and 12-μm radiances to retrieve cirrus, often referred to as the split-window method, was originally explored by several researchers (Inoue 1985; Wu 1987; Prabhakara et al. 1988). Further studies by Parol et al. (1991), Giraud et al. (1997), and Luo et al (2002) discussed the sensitivity of the method to the microphysical properties of cirrus. More recently, Cooper et al. (2003) used the split-window method in an optimal estimation framework. Here, we briefly describe our version of the method and its application to satellite data. More details concerning the derivation of the split-window method and an uncertainty assessment can be found in the Luo (2003).

The split-window method can be formulated as

$$I_{\text{obs}}^{11} = (1 - \varepsilon_{\text{eff}}^{11})I_{\text{clr}}^{11} + \varepsilon_{\text{eff}}^{11}B^{11}(T_c), \tag{1}$$

$$I_{\text{obs}}^{12} = (1 - \varepsilon_{\text{eff}}^{12})I_{\text{clr}}^{12} + \varepsilon_{\text{eff}}^{12}B^{12}(T_c), \quad \text{and} \tag{2}$$

$$\frac{\varepsilon_{\text{eff}}^{12}}{\varepsilon_{\text{eff}}^{11}} = f(T_c) = g(r_e), \tag{3}$$

where I_{obs}^{11} and I_{obs}^{12} denote the satellite-observed radiances at 11 and 12 μm, and I_{clr}^{11} and I_{clr}^{12} denote the corresponding clear-sky radiances (including the effects of the surface and atmosphere). Here, $B^{11}(T_c)$ and $B^{12}(T_c)$ represent the blackbody radiances for the cloud-top temperature T_c (for optically thin clouds; this is really the layer mean temperature), and $\varepsilon_{\text{eff}}^{11}$ and $\varepsilon_{\text{eff}}^{12}$ are the cloud effective emissivities at 11 and 12 μm, whose ratio is a function of the cloud microphysics [Eq. (3)]. Equations (1)–(3) constitute a simple and complete cloud model from which T_c, $\varepsilon_{\text{eff}}^{11}$ and $\varepsilon_{\text{eff}}^{12}$ can be retrieved. See Luo (2003) for a derivation of these equations.

The split-window method has not yet been used to produce a global, long-term, and high spatial/temporal resolution cirrus dataset suitable for climate study. In this study, 3 yr of split-window data (1996–98) were produced following the approach described above. Since the ISCCP DX data product includes both the 11- and 12-μm radiances when available, we can build the split-window cirrus dataset upon the existing ISCCP product to take full advantage of the various analysis results provided by ISCCP. For example, ISCCP conducts a series of spatial/temporal analyses to determine clear/cloudy condition for each pixel. Moreover, ISCCP saves the clear-sky radiances for each pixel. These clear-sky analyses provide information for solving Eqs. (1)–(3) and also help minimize uncertainties associated with the clear-sky estimation. See Luo (2003) more details. In total, three geostationary [*Geostationary Meteorologi-*

cal Satellite-5 (*GMS-5*), and *Geostationary Operational Environmental Satellite-10* (*GOES-10*) and *-8* (*GOES-8*)] and two National Oceanic and Atmospheric Administration (NOAA) polar-orbiting satellites have the split-window channels in the late 1990s. However, we only use the two polar orbiters (*NOAA-12* and *NOAA-14*) in this study to produce a dataset with roughly 6-hr temporal resolution and 4-km spatial resolution (at nadir, sampled to 30-km intervals by ISCCP). We chose the 6-hourly temporal sampling, rather than the 3-h sampling over the regions observed by GOES and GMS satellites, to match the time intervals of the NCEP–NCAR reanalysis winds used in the Lagrangian analysis of cirrus evolution discussed in section 4. Moreover, use of two NOAA polar orbiters minimize errors and inconvenience having to do with intersatellite calibration.

b. *ISCCP cloud analysis scheme and product*

ISCCP analyzes infrared ($\approx$11 μm) and visible ($\approx$0.6 μm) radiances measured by the imaging instruments on all of the operational weather satellites. The cloud analysis procedure in ISCCP consists of three principle steps: cloud detection, radiative model analysis, and statistical analysis (Rossow and Schiffer 1991). Cloud detection is achieved by first constructing a clear-sky radiance map and then applying a threshold to detect clouds (Rossow and Garder 1993). After cloudy pixels are separated from clear pixels, cloud radiative properties are determined by comparing the observed visible reflectance and infrared brightness temperature with the radiative model calculations; at night only the IR is available so all clouds are treated as blackbodies. Clouds are represented in the radiative model as a single, physically thin layer, uniformly covering the image pixel with a specified particle size distribution. When cloud optical thickness is small enough (such as for cirrus), such that a significant portion of radiation from the surface and atmosphere below is transmitted, the retrieved value of cloud-top temperature (T_c) is reevaluated using visible radiances in daytime to account for this transmission. For clouds colder than 260K, the cloud microphysical model is an ice cloud composed to 30-μm polycrystals (Rossow and Schiffer 1999). Clouds are then classified in ISCCP according to cloud-top pressure (P_c) and optical thickness (TAU) as shown in Fig. 1.

c. *Comparison of cirrus from ISCCP and the split-window analysis*

Following the classification in ISCCP, cirrus are defined as clouds with cloud-top pressure (P_c) < 440 mb and TAU < 3.6. We also discuss a cloud category called cirrostratus, clouds having P_c < 440 mb and 3.6 < TAU

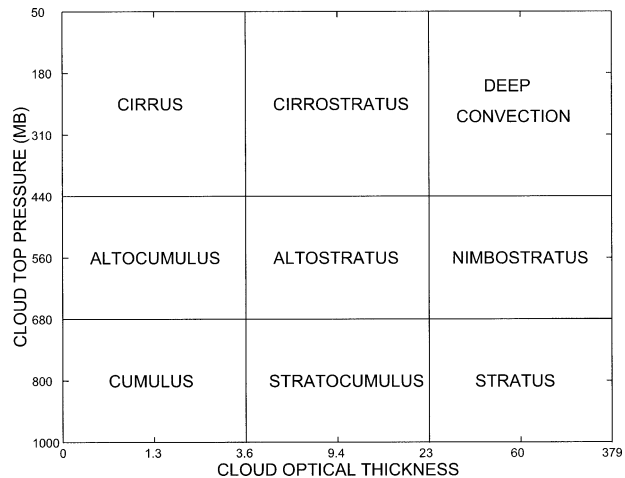FIG. 1. Cloud classification in the ISCCP D-series dataset.

< 9.4.[3] First, we show in Fig. 2 the monthly mean cirrus amount (from the split-window retrieval) and deep convective cloud amount (from ISCCP) for January and July of 1996. Generally, tropical cirrus are located in the regions where convective activity is frequent and moisture is abundant: the tropical warm pool, tropical Africa, the Amazon, the ITCZ, and the South Pacific Consequence Zone (SPCZ). Jin et al. (1996) also note that the thinnest cirrus missed by ISCCP exhibit a similar geographical pattern to the cirrus detected by ISCCP. The eastern Pacific and subtropics are generally cirrus free. Despite the similar geographical patterns of cirrus and deep convection in the monthly mean map, they may not be as closely related in an instantaneous sense when tracking the origin and evolution of these two types of clouds. We will get back to this in the next two sections, but we point it out here to caution against the simple interpretation of monthly mean maps.

Figure 3 shows the comparison of zonal monthly mean cirrus frequency from the ISCCP and the split-window method. Over ocean, the split-window method and the ISCCP identify almost the same amount of cirrus: the difference is generally smaller than about 0.02. Over land, however, the difference is a little larger (about 0.05) and varies with latitude: ISCCP identifies less cirrus over the deep Tropics (rain forest) but more over the subtropics (desert regions). Luo (2003) evaluated cirrus retrieved by ISCCP and the split-window method by using a third-party observation, namely, an analysis of the collocated radiance measurements from the infrared (6.7 μm) and microwave (183 GHz) water vapor channels. It was suggested that both methods are

---

[3] Note this differs slightly from ISCCP where cirrostratus are defined as cloud with P_c < 440 mb and 3.6 < TAU < 23. TAU is cut off at 9.4 because the split-window retrieval of TAU saturates about there. In other words, the split-window method cannot differentiate TAU at 9.4 from much larger values. The same is true for most other infrared-based retrieval methods.
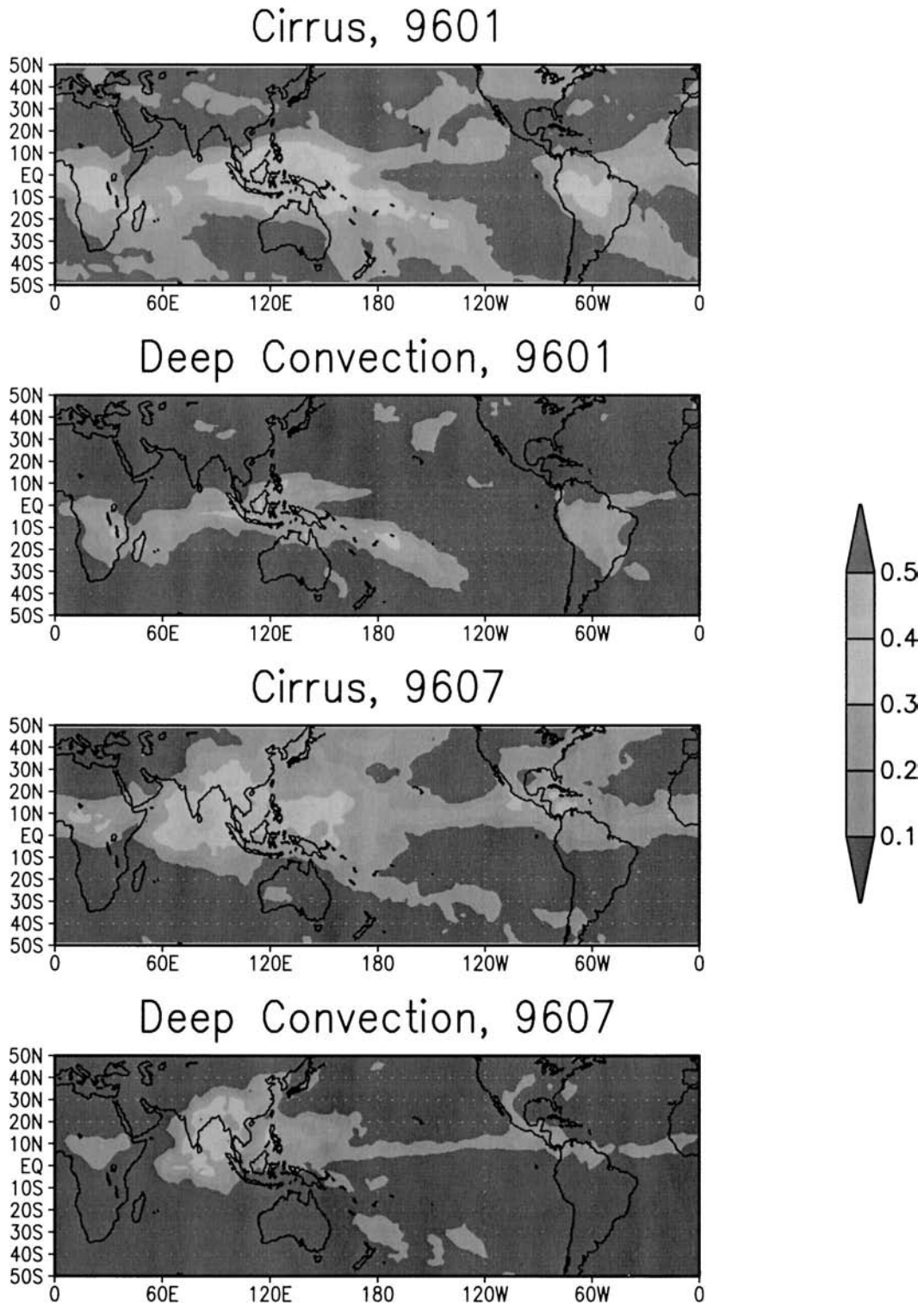
FIG. 2. Monthly mean cirrus amount from the split-window method and the deep convective cloud amount from ISCCP for Jan and Jul 1996.
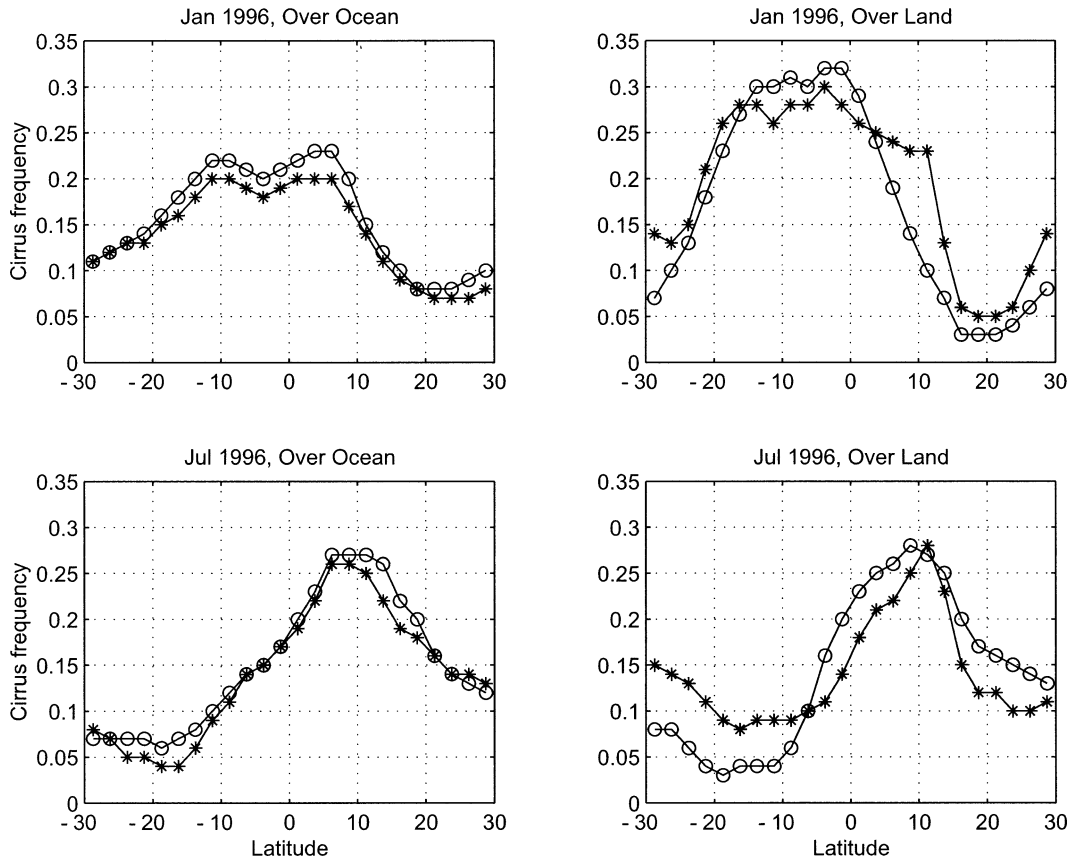
FIG. 3. Comparison of zonal mean cirrus amount from the split-window analysis (open circles) and ISCCP (stars).

capable of correctly retrieving cirrus properties as long as they are optically thick enough (TAU > 1). Possible reasons for discrepancies in Fig. 3 are that ISCCP misidentifies cirrus overlying lower-level clouds in active convective regions, while the split-window method has some difficulty dealing with the variation of land surface emissivity. The extra "cirrus" in the ISCCP results over deserts may also be misidentified dust storms. Very thin cirrus can be detected even though their brightness temperatures are not very different from clear sky, but they are not readily put at the right altitude (cf. Luo et al. 2002).

One major difference between the two cirrus schemes is that the split-window method uses two infrared radiances and the ISCCP cloud scheme uses one visible and one infrared radiance. As a result, cirrus information is available only for the daytime part of the world in ISCCP data. The split-window analysis, on the other hand, can be applied to retrieve cirrus both day and night. Since the main purpose of analyzing the satellite cirrus dataset in this paper is to study their evolution processes and life cycle, the frequent and continuous availability of observations is critical; using ISCCP data might miss some stages of cirrus evolution. Therefore, the following analyses are limited to cirrus from the split-window method, except one figure that shows the

influence of the tropical circulation on the cloud-type distribution.

d. The upper-tropospheric water vapor data

The upper-tropospheric water vapor (UTWV) or the upper-tropospheric humidity (UTH) is derived from the radiance measurements from the Special Sensor Microwave Temperature 2 (SSM/T2). The SSM/T2 is an operational passive microwave water vapor sounder on board the Defense Meteorological Satellite Program (DMSP) satellites (Falcone et al. 1992), consisting of five channels: three water vapor channels centered around the 183.31-GHz water vapor resonance lines at 183 ± 1, 183 ± 3, and 183 ± 7 GHz, and two window channels at 91.665 and 150.0 GHz. In this study, radiances from the 183 ± 1 GHz channel, which are sensitive to moisture above 500 mb, are used to retrieve the UTWV or UTH.[4] Most previous studies have used infrared upper-tropospheric water vapor radiances

---

[4] We use the terms UTWV and UTH to mean the vertically weighted upper-tropospherc specific humidity (g kg^{-1}) and relative humidity (%) respectively. The layer over which the UTWV and UTH are derived is roughly from 500 to 200 mb and we call it the UTWV layer.
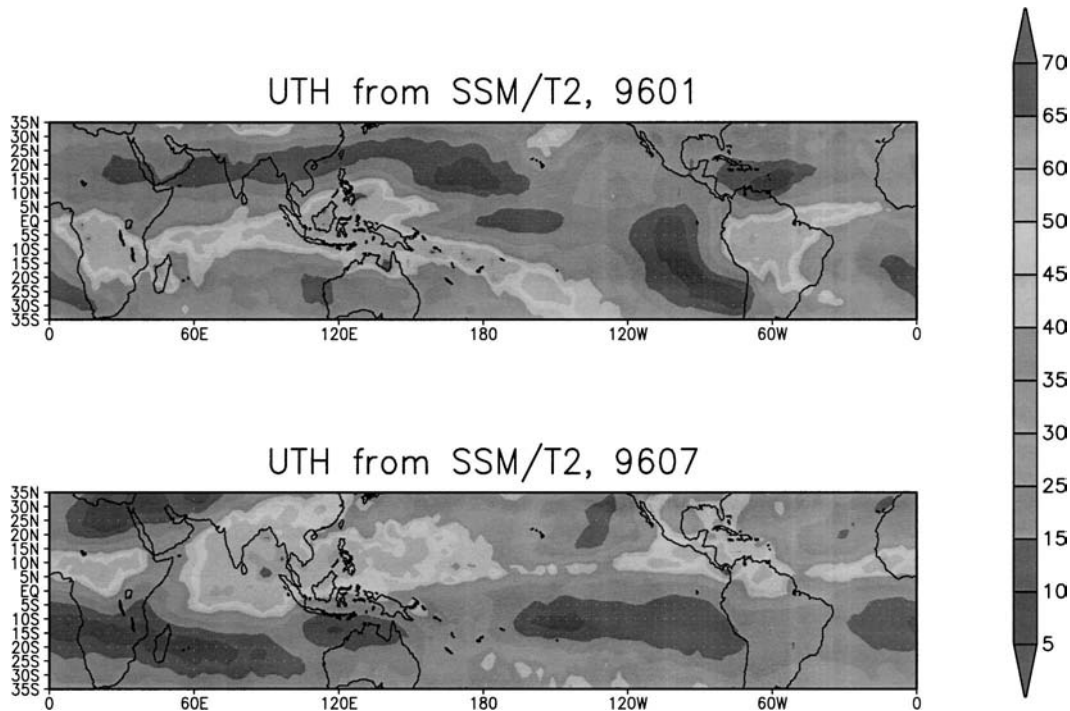
FIG. 4. UTH retrieved from SSM/T2 for Jan and Jul 1996.

(UTRs), at 6.7 μm, to derive UTWV information. However, IR UTRs are strongly affected by high clouds. Since high clouds cover at least 0.25 of the Tropics (with cirrus being the most frequent form), UTWV based on IR UTRs would either leave these regions unsampled if strict cloud clearing is applied or yield biased results if cloud clearing is not applied. Microwave UTRs, on the other hand, are insensitive to nonprecipitating ice clouds such as cirrus (Greenwald and Christopher 2002); cloud contamination becomes a serious issue only for precipitating cold clouds, which cover a much smaller fraction of the Tropics (<0.05) where air is probably close to saturation anyhow. Therefore, UTWV retrieved from microwave UTRs provides much more complete coverage than that from the IR.

In cloud-free regions, however, IR and microwave UTRs are highly correlated, differing a little because of different sensitivities to temperature variations and slightly different vertical weighting functions (Berg et al. 1999). Therefore, we develop our microwave UTWV or UTH retrieval by regressing IR UTRs against microwave UTRs in clear scenes (as determined by ISCCP) and then use the UTWV versus IR UTR relationship, calculated from a radiative transfer model Streamer (Key 1996), as a bridge to derive the relationship between UTWV and microwave UTRs. The data used in this analysis are 2 months of ISCCP DX results collocated with SSM/T2 at pixel level. The ISCCP data are from *GOES-9, GOES-10,* and *Meteosat-7,* all of which have a 6.7-μm channel. For relative humidity UTH with respect to liquid water (note that

values are 30%–40% higher with respect to ice), this relationship is

$$\ln(\text{UTH}/\cos\theta) = -0.084\,06 \times \text{TBB}_{183\text{GHz}} + 24.32, \quad (4)$$

where $\text{TBB}_{183\text{GHz}}$ is the observed brightness temperature at 183 ± 1 GHz and θ is the satellite viewing angle. This equation looks similar to the one used by Soden and Bretherton (1993) and Engelen and Stephens (1998), but uses microwave UTRs from 183 GHz with different coefficients to translate from infrared to microwave radiances. Following the approach by Moody et al. (1999), a similar relationship can be derived for retrieving UTWV in terms of specific humidity:

$$\ln(\text{UTWV}/\cos\theta) = -0.084\,06 \times \text{TBB}_{183\text{GHz}}$$
$$+ 0.084\,06 \times \overline{T} - 7.8994, \quad (5)$$

where $\overline{T}$ represents the average upper-tropospheric layer temperature. The temperature data are from the operational NOAA TOVS retrievals, which are saved in the ISCCP D1 product (Rossow et al. 1996). Figure 4 shows the monthly mean UTH retrieved from this algorithm. Note the similar patterns between Figs. 2 and 4.

Possible uncertainties associated with the UTWV (UTH) retrieval method described above come from the difference between IR and microwave UTRs which have different sensitivities to temperature variations and slightly different vertical weighting functions. We have reduced the uncertainty associated with the original IR treatment by using the stricter ISCCP cloud clearing. One measure of the IR–microwave differences is the

standard deviation associated with the regression of $TBB_{6.7\mu m}$ against TBB_{183GHz} in clear scenes. Two months of data (January and July 1996) are used to compute the regression relation between $TBB_{6.7\mu m}$ and TBB_{183GHz} the standard deviation is about 2 K. From Eq. (4), an error of 2 K in TBB_{183GHz} produces an absolute error of 5% in UTH values near 30% and 10% in UTH values near 60%. So, the relative magnitude of this error is about 17% for UTH values from 30% to 60%, the range observed in section 6 where we discuss the relationship between cirrus and UTWV. Since this error occurs randomly, there should be no systematic bias in the retrieval of UTWV (UTH). Another source of error comes from the TOVS temperature profile when specific humidity UTWV is retrieved using Eq. (5). Stubenrauch et al. (1999a) compared the difference between temperature profiles from the operational TOVS and the improved initialization inversion (3I) retrieval: the former is warmer than the latter by less than 0.5 K in the tropical upper troposphere. Kidder and Vonder Haar (1995) analyzed the biases and rms differences in temperature between TOVS and radiosonde soundings: for tropical regions, the bias was found to be less than 0.4 K and the rms difference to be about 2 K in the upper troposphere. So, the magnitude of the uncertainty from the TOVS temperature profile is comparable to that from the regression between $TBB_{6.7\mu m}$ and TBB_{183GHz}. Note that the main purpose of examining UTWV (UTH) in this study is to understand its evolution, so the relative accuracy of the retrieval is more important. Discussion of a more rigorous retrieval of UTWV can be found in Engelen and Stephens (1999).

3. The Lagrangian forward trajectory method

A forward-trajectory analysis is the basis for determining cirrus life cycle, evolution, and relation to the upper-tropospheric water vapor. The main assumption is that cirrus, like other tracers (e.g., water vapor), drift with the upper-tropospheric wind, while at the same time, going from formation to maturation to decay. Trajectories of air parcels are constructed using upper-tropospheric winds obtained from the NCEP–NCAR reanalysis, which is based (in part) on satellite cloud drift winds (Kalnay et al. 1996) that use the same assumption. Thus, cirrus cloud evolution is tracked by keeping a record of its various stages and the UTWV along these trajectories. A similar method has been employed to study marine stratus clouds (Bretherton and Pincus 1995; Pincus et al. 1997) and upper-tropospheric humidity (Salathe and Hartmann 1997, 2000) regionally. But extending the trajectory method to the global scale and applying it to cirrus have not been tried before.

Since the temporal and spatial sampling intervals of the NCEP–NCAR reanalysis wind are 2.5° and 6 h, respectively, we are unable to track the life cycle of any specific piece of cirrus cloud. Instead, we calculate the cirrus amount, as well as average cirrus properties (P_c

and TAU), within each 2.5° by 2.5° grid box for every 6-h time step. We assume cirrus amount is a good indicator of its life cycle. For example, cirrus lifetime can be measured as the duration along a trajectory (or part of a trajectory) that exhibits a sequence from zero cirrus to some amount of cirrus to zero cirrus again. For cirrus formed by convective detrainment, cirrus amount monotonically decreases (after a start-growth phase) until it vanishes.

The forward air trajectories considered in this study start from deep convective events, which are defined as the last grid box in a time sequence that has more than 0.10 deep convective cloud cover. In other words, it has to meet the following two conditions: 1) it has more than 0.10[5] deep convective cloud cover (cloud-top temperature T_c less than the temperature at 180 mb or roughly 220 K), and 2) its downstream boxes have less than 0.10 deep convective cloud cover. Requiring T_c to be less than 220 K is a more stringent definition of tropical convective systems than in previous studies (cf. Salathe and Hartmann 1997) and corresponds more to the convective core of these systems (cf. Machodo and Rossow 1993). The rational for starting the trajectories close to the convective core is to sample the whole transition from deep convection to thick anvil to cirrostratus and finally to cirrus. Starting the trajectories from convective systems does not mean that we assume all cirrus are derived from convection, since we also allow cirrus to re-form along the trajectories. Initiating trajectories from where convection dies out provides a convenient way of comparing cirrus formed from convective detrainment to cirrus formed in situ. As will be shown in the next section, cirrus from convective detrainment generally do not last for more than about 1 day. Thus, cirrus seen several days after a convective event are not likely derived from convection, although the trajectories along which we search for cirrus start from the convection (some of the water vapor to form in situ cirrus may come from the convection, however). The distinction between cirrus generated by convection and cirrus formed in situ will become clearer in the next section. Moving along a forward trajectory, convective activity can sometimes last for several 6-h time steps (cf. Machado et al. 1998). In this case, the last time step is considered to be the decay stage of the convective system and our search for cirrus starts from there. If a forward trajectory encounters another convective system along the way, we terminate this trajectory and start a new one from there.

One compromise we need to make, given the uncertainty and variation of cirrus cloud-top height and the coarse resolution of the UTWV, is to average the wind field over the whole air column between 500 and 200

---

[5] By choosing this threshold, we are limited to the convective systems larger than about 50 km in radius. A convective system whose radius is smaller than 50 km will cover less than 0.10 of the grid box as used in ISCCP (280 km by 280 km).
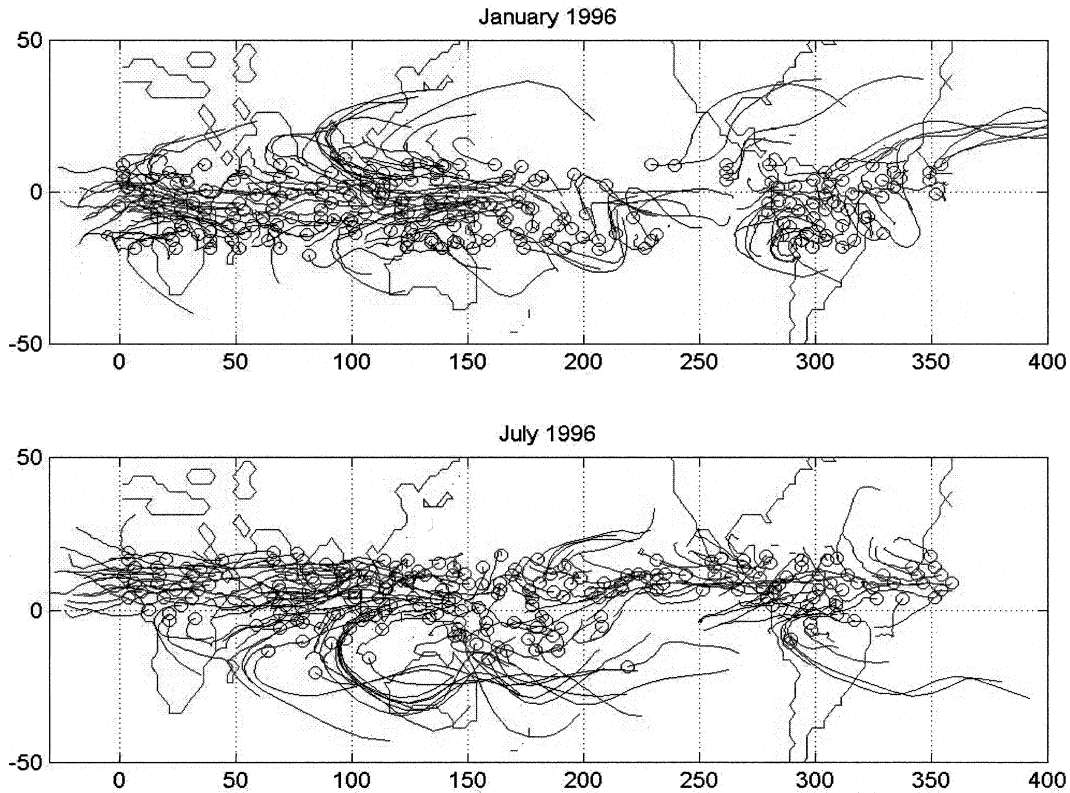
January 1996

July 1996

FIG. 5. Examples of Lagrangian forward air trajectories. Circles represent the starting points of each trajectory. Note that the eastern Pacific has much fewer trajectories because very little convection occurs there.

mb and use it to represent the upper-tropospheric wind. Vertical movement of air masses is not examined explicitly because we do not know the quality of the vertical wind from the reanalysis. So, we are considering the two-dimensional movement of the air columns within the 500–200-mb layer. A similar approach was taken by Pincus et al. (1997) and Salathe and Hartmann (1997). Because of this limitation, we only follow a forward air trajectory for a maximum of 5 days because after 5 days, the air column between 500 and 200 mb may well have subsided into a lower level (given a climatological clear-sky subsidence rate in the Tropics of about 30 mb day^{-1}). In fact, since we terminate a trajectory when it encounters another convective system along the way and start a new one from there, about 70% of the trajectories in our study are shorter than 5 days: the average length is around 3 days.

Figure 5 shows examples of the forward air trajectories from January and July of 1996. The usual centers of convective activity are evident in the figure: tropical western Pacific, tropical Africa, and the Amazon. Upper-tropospheric air parcels start from these convective centers and make their way into the subtropics or tropical dry regions (such as the eastern Pacific). It is also interesting to see that some of the air parcels, mostly in the winter hemisphere, are picked up by subtropical

jet streams and travel a longer distance over the 5-day period.

4. Variation of tropical cirrus along forward trajectories

a. Lagrangian view of the influence of the tropical circulation on cloud property distributions

Following the forward air trajectories, cloud properties (or cloud types) undergo a systematic change. Figure 6 shows the cloud property distribution from ISCCP (daytime only) in terms of P_c and TAU (see Fig. 1) for the convective source regions and for 5 days following the last convection. As air makes its way from convective regions to dry regions, it travels from a place where high, thick clouds prevail, to a place where cirrus and low-level clouds dominate. This is consistent with the traditional picture of the Hadley/Walker circulation concerning how the large-scale circulation influences clouds, except that Fig. 6 shows the influence from a Lagrangian trajectory perspective. Rather than treating convective centers (such as the ITCZ) only in the time average, we consider intermittent convective systems with scales of a few hundred kilometers, which are separated by relatively clear and dry regions. Cirrostratus and thicker cirrus, which are prevalent close to the con-
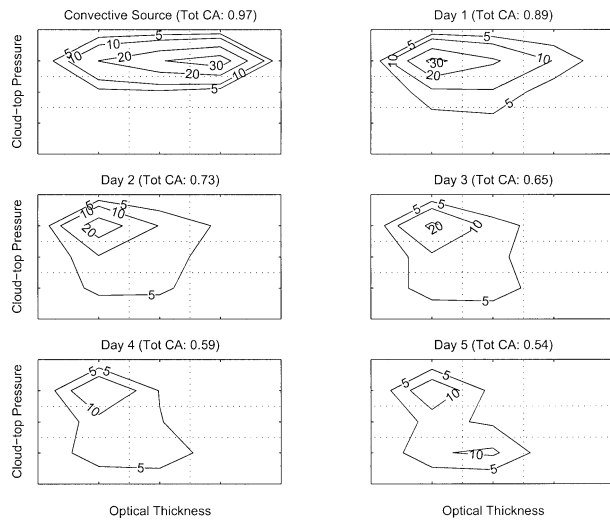
FIG. 6. Cloud property distributions (see Fig. 1) along forward air trajectories sorted by the number of days air has traveled from the last convection. The contour levels are cloud amounts. The dashed lines correspond to the ISCCP cloud classification (e.g., the upper three boxes from the left to the right correspond to cirrus, cirrostratus, and deep convection, respectively). Total cloud amount is shown in the parentheses on top of each subplot.

vective regions (lasting only about 1 day), become less and less frequent as air moves into dry regions. On the other hand, low-level clouds become important several days after air leaves the convective regions and continue to grow more and more prevalent. Note that that obscuration of low clouds by high clouds is not likely a serious issue, except within the convective regions, because most of the high clouds shown from day 1 to day 5 are cirrus, which would not be so identified if low clouds coexisted below them (cirrus overlapping low clouds are most likely identified as middle-level clouds by the ISCCP cloud scheme). Total cloud amount drops from 0.97 in the convective source regions to 0.54 on the fifth day (shown on top of each subplot). The high-level cloud amounts for the source region, day 1, and all the way to day 5 are 0.86, 0.64, 0.40, 0.32, 0.25, and 0.20, respectively, of which convective cloud amounts are 0.36, 0.10, 0.04, 0.03, 0.02, and 0.02, respectively.

b. The evolution of tropical cirrostratus and cirrus

Jin (1998) studied the temporal autocorrelations for different high cloud types. Her results suggested that cirrus are stationary while medium thick high-level clouds propagate together with deep convection, implying that not all cirrus are produced and maintained by the same processes as are medium and thick high-level clouds. Jin et al. (1996) found similar geographic patterns for the cirrus detected and missed by ISCCP, but Wang et al. (1996) show that the latter occur systematically higher than the former. The temporal autocorrelation method reveals the temporal evolution patterns

of clouds in an Eulerian perspective. In this study, we look at the evolution of cirrus by following the movement of the air leaving the vicinity of convective systems and examine the variation of cirrus along the forward air trajectories. Figure 7 shows the averaged cirrus/cirrostratus cloud amount, cloud-top pressure, and optical thickness as a function of time from last convection along forward trajectories (see section 2c for the definition of cirrus and cirrostratus) from the split-window analysis. Data from January and July 1996 are used and altogether 7748 trajectories are composited.

Several important features are illustrated in Fig. 7 concerning the evolution of cirrus and cirrostratus. 1) The decay of deep convection is rapid (6–12 h),[6] and is associated with the growth of both cirrostratus and cirrus. The time and spatial scales of the transition from convection to cirrostratus (probably as convective detrainment) are about 6 h and 200 km, respectively. The decay of cirrostratus is then accompanied by the continued growth of cirrus, indicating a decay of cirrostratus into cirrus. From the decay of cirrostratus, it takes another 6 h for the cirrus amount to reach its peak. Because of the 6-hr time step employed, the average time for these changes may be smaller; however, the rapid evolution of smaller convective systems is not included because we require 0.10 area coverage in 2.5° grid cells to identify these systems (see discussion in Machado et al. 1998). 2) The relatively rapid decay of cirrostratus over about 500–700 km or 1 day downstream of convection suggests a loss of cloud water mass. Note that cirrostratus most likely form by the convective detrainment and/or as part of an associated mesoscale circulation and contain a much larger water mass (and larger particles than cirrus) and consequently have much larger sedimentation mass flux. Since the upper troposphere monotonically dries out as cirrostratus decay away (see section 6 for details) and the time scale for cirrostratus decay is much longer than estimates for ice particle lifetimes (less than an hour for big particles in cirrostratus; see section 7 for an estimation of particle sedimentation rate), the evolution of the cirrostratus is probably not a simple sedimentation loss of water or a simple evaporation, but a more complex interaction of rapid sedimentation to lower levels (as suggested by the increasing cloud-top pressure), opposed by a dynamical supply of water vapor from below (mesoscale circulation) and a dispersal of water as the area expands (cirrostratus typically cover 2–3 times the area of the convective towers). 3) Cirrostratus being at a lower pressure (higher level) than cirrus suggests that the transition from cirrostratus to cirrus is accompanied by a gradual decrease in cloud-top height. The evolution of cirrus properties also indicates that cirrus tend to thin out and move to the lower levels, as air moves away from con-

---

[6] This is not the lifetime of convection (cf. Machado et al. 1998) because we start from the last time when the convective cloud amount exceeds 0.10.
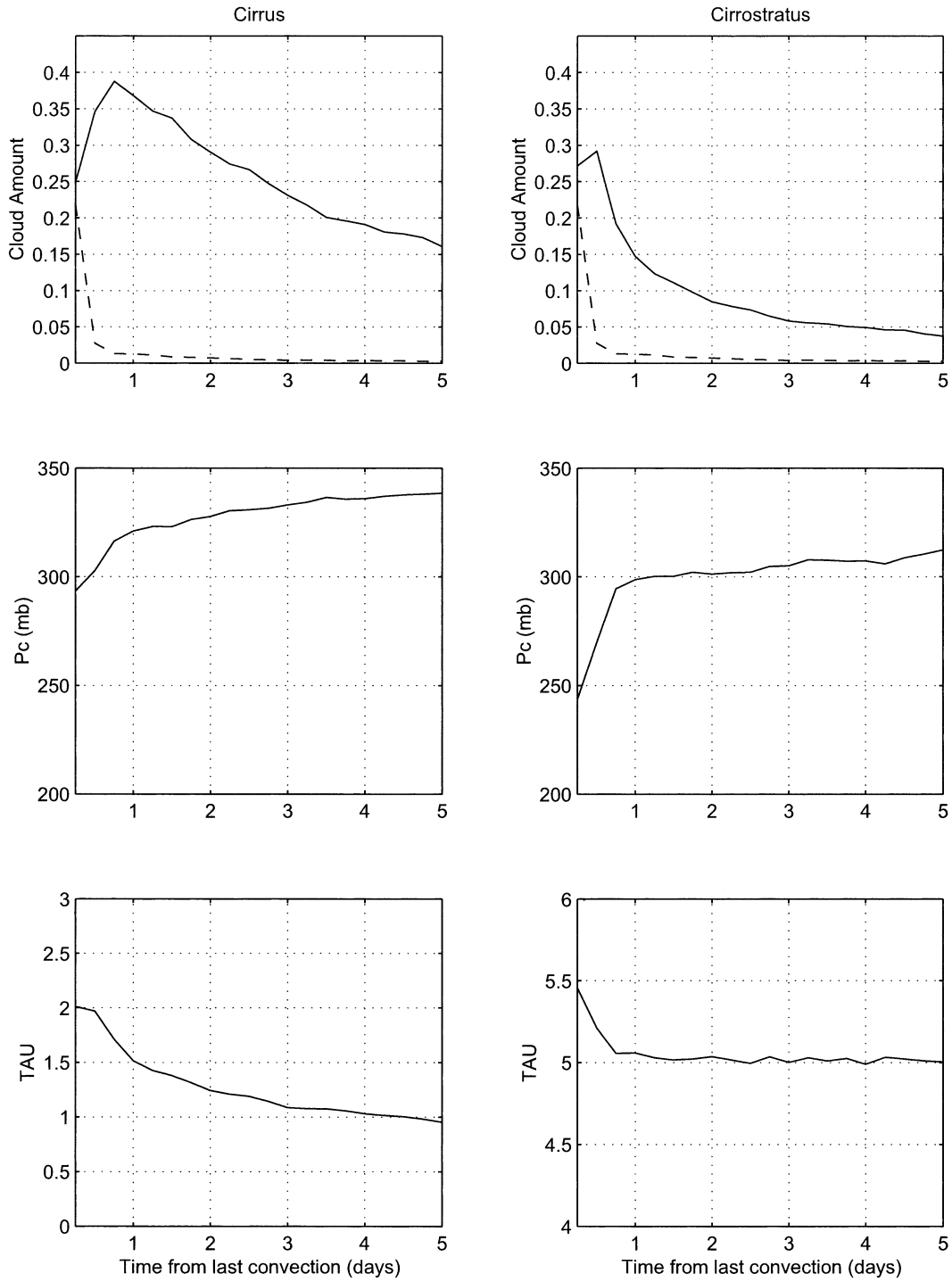
FIG. 7. Average cirrus/cirrostratus cloud amount, cloud-top pressure (P_c), and optical thickness (TAU) as a function of *time* from last convection along forward trajectories. Results shown are from the split-window retrieval (see section 2c for definitions of cirrus and cirrostratus). The dashed lines in the upper two subplots are the deep convective cloud amounts (see section 3 for the definition of deep convective clouds).

tropical Africa

Indian and west Pacific warm pool
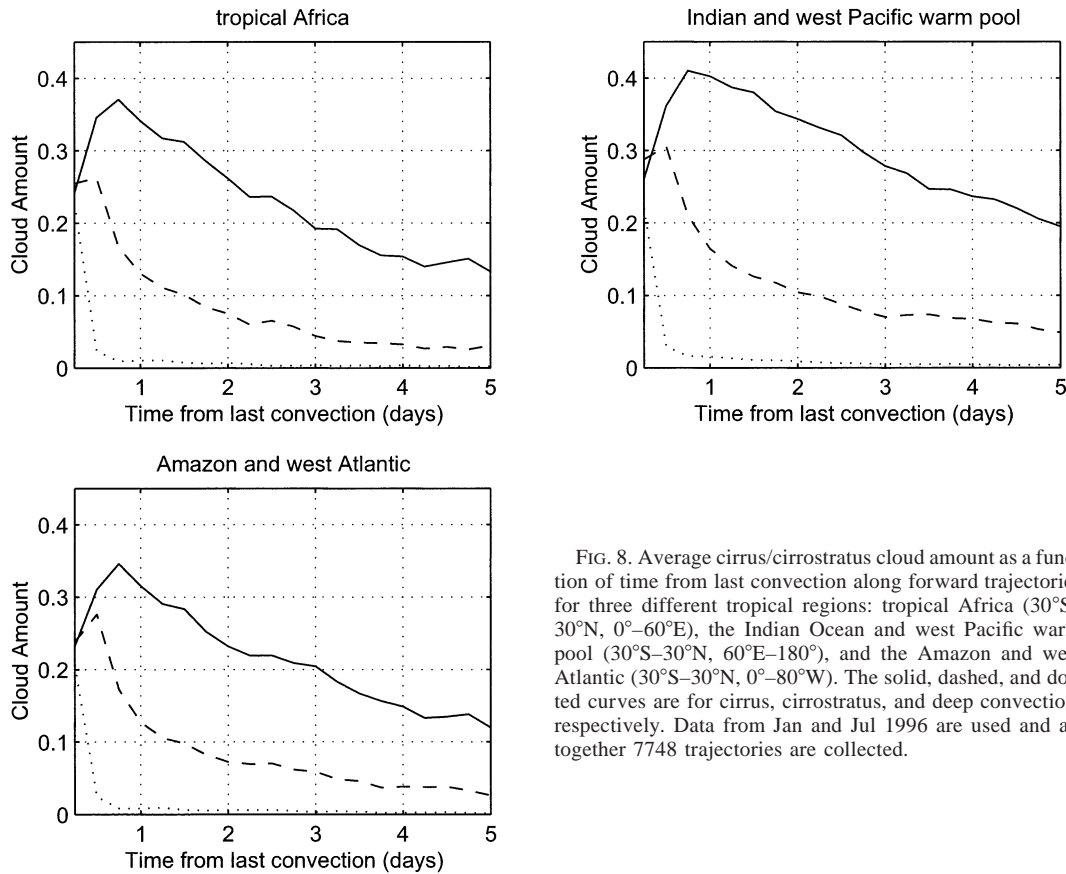

Amazon and west Atlantic

FIG. 8. Average cirrus/cirrostratus cloud amount as a function of time from last convection along forward trajectories for three different tropical regions: tropical Africa (30°S–30°N, 0°–60°E), the Indian Ocean and west Pacific warm pool (30°S–30°N, 60°E–180°), and the Amazon and west Atlantic (30°S–30°N, 0°–80°W). The solid, dashed, and dotted curves are for cirrus, cirrostratus, and deep convection, respectively. Data from Jan and Jul 1996 are used and altogether 7748 trajectories are collected.

vective regions. 4) Cirrus amount decreases more slowly along forward trajectories than cirrostratus: the *e*-folding time is longer than 5 days for cirrus, while it is about 1–2 days for cirrostratus. This is consistent with Jin's finding that cirrus and cirrostratus are most likely produced and maintained by different processes. That is, convective detrainment is probably not the only source for producing and maintaining cirrus. Other dynamics processes (e.g., vertical transport of water vapor by waves or large-scale uplifting) also exist that could be responsible for their formation and maintenance. Jensen et al. (2001a,b), for example, discussed the theoretical and observational aspects of some optically very thin cirrus around the tropical tropopause, which are frequently observed to exist without other thick high clouds nearby. We will return to this topic in section 6.

There are some regional differences associated with the Lagrangian evolution of tropical cirrus. Figure 8 shows the evolution of cirrus, cirrostratus, and deep convective cloud amount for three tropical regions where cirrus are frequently seen: tropical Africa (30°S–30°N, 0°–60°E), the Indian Ocean and west Pacific warm pool (30°S–30°N, 60°E–180°), and the Amazon and west Atlantic (30°S–30°N, 0°–80°W). Cirrus and cirrostratus amounts are greater in the Indian Ocean and west Pacific warm pool than in the other two regions, but the decay

rate is similar for all three regions. More frequent convective activity and upward motions in the warm pool are probably responsible for greater cirrus/cirrostratus amounts. The evolution of cirrus properties such as P_c and TAU, on the other hand, does not exhibit a noticeable regional variation (not shown). We also sort cirrus properties and their evolution by the strength of the convective sources, which is not shown in this paper but can be found in Luo (2003). Stronger convective systems (defined as having colder cloud tops) correspond to higher cirrus tops, larger cirrus optical thicknesses, but similar cirrus decay rates. Regardless of the convective strength, cirrus tops generally stabilize at around 300 mb about 1 day after air leaves the convective region and does not have much memory of the convective strength after that. Cirrus optical thickness seems to have a slightly longer memory (about 2 days).

c. Tropical cirrus lifetime and advection distance

Figures 7 and 8 give us a general sense of how tropical cirrus evolve along forward trajectories. Nevertheless, they are not enough to characterize the cirrus life cycle because compositing over many trajectories smears out the detailed life cycle of each individual trajectory. For example, we cannot quite tell from Fig. 7 what is the
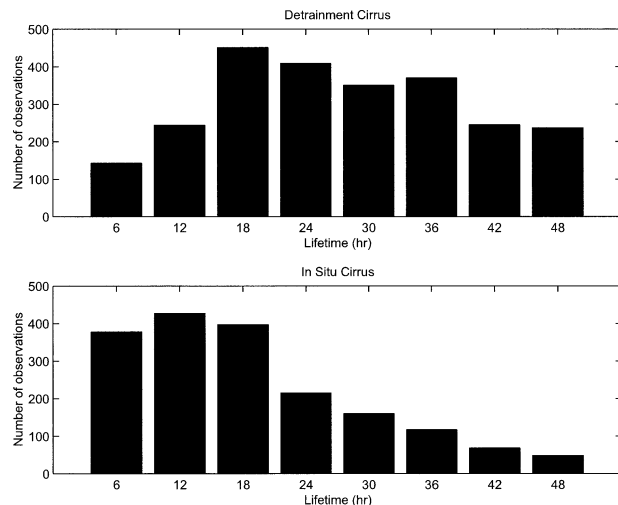
FIG. 9. Histograms of cirrus lifetime for (top) detrainment cirrus and (bottom) in situ cirrus.

typical lifetime of tropical cirrus systems. Although the composite picture shows that is takes a little more than 5 days for cirrus amount to *e*-fold, an individual cirrus system may have a much shorter life cycle. Therefore, in this section we take a different approach toward characterizing tropical cirrus lifetime by collecting statistics from each individual trajectory.

Due to the temporal and spatial resolutions of the NCEP–NCAR reanalysis (2.5° and 6 h, respectively), we assume that the cirrus cloud fraction is a good indicator of cirrus evolution. In other words, we assume that the life cycle is characterized along a trajectory by the systematic variation of cirrus cloud amount. We consider two types of tropical cirrus based on their relationship to convective systems: detrainment cirrus and in situ cirrus. The life cycle for detrainment cirrus is defined by a monotonic decrease of cirrus amount along a forward trajectory like this: last convection becoming some cirrus becoming zero cirrus. The length of this sequence defines the detrainment cirrus lifetime. For in situ cirrus, the sequence is appearance of cirrus with first an increase and then a decrease of cirrus amount like this: zero cirrus (observed at least 1 day after convection) becoming some cirrus becoming zero cirrus. The requirement that the air parcel encounter clear skies after convection ensures the separate evolution of the in situ cirrus.

Figure 9 shows the histogram of cirrus lifetimes for both detrainment and in situ cirrus. The lifetime for detrainment cirrus is about 30 ± 16 h. The shape of the histogram suggests that there are few lifetimes shorter than 6 h, which cannot be resolved in our data; however, our definition of convection excludes the smallest systems (cf. Machado et al. 1998). Including the smallest systems could reduce the average lifetime somewhat. For in situ cirrus, the lifetime is about 19 ± 17 h. The shape of this histogram suggests that there may be more

in situ cirrus with lifetimes <6 h, however, even if the amount of this cirrus is comparable with that at 6 h, the average lifetime could only be reduced by 2–3 h.

Because we look at relatively large areas (2.5° by 2.5°; about 77 000 km²), the definition of "zero cirrus" needs to be relaxed from absolute zero; otherwise, we would have very few samples of distinct cirrus life cycle sequences. In practice, we take zero cirrus to be 1/5 of the maximum cirrus cloud amount along the lifecycle sequence. For example, when cirrus overcast decays below 0.20, we call this the end of the life cycle. But if the maximum cirrus amount along a selected trajectory is only 0.20, then it has to drop below 0.04 to end the life cycle. The average maximum cirrus amount along the trajectories in this study is 0.61. We tested the sensitivity of our results to the choice of zero cirrus by trying different definitions, such as 1/10 of the maximum cirrus amount: a similar distribution of cirrus lifetimes with a mean value about 2–4 h longer is obtained. Compared to the lifetime of tropical convection (Machado et al. 1998), tropical cirrus have a longer duration and a larger standard deviation. The large spread in lifetimes suggests that a wide variety of mechanisms may be responsible for the generation and maintenance of tropical cirrus.

Finally, we examine how far tropical cirrus travel with the upper-tropospheric wind during their life cycle. The advection distance of tropical cirrus derived from the average of each cirrus trajectory shows a linear relationship: for each 6-h time step, tropical cirrus travel roughly 200 km, which corresponds to an average wind speed of about 10 m s⁻¹. Hence, for an average cirrus lifetime of 30 h (detrainment cirrus) and 19 h (in situ cirrus), tropical cirrus advect about 600–1000 km during their lifetimes, which spans many grid boxes for most current GCMs.

5. Detrainment cirrus versus in situ cirrus

In the previous section, we distinguished between detrainment cirrus and in situ cirrus based on their relationship to convective systems. Now, we ask how many tropical cirrus are derived directly from convective detrainment and how many are produced in situ. Heymsfield and Donner (1990) estimated the frequency of observing cumulonimbus and cirrus simultaneously and found that from 30°S to 30°N, the annual average percentage of cirrus occurring simultaneously with cumulonimbus is 17% over ocean and 12% over land. Although their results are relevant to the question framed here, they do not provide an unambiguous answer because they did not follow a cirrus life cycle and could not determine where to draw the line between detrainment cirrus and in situ cirrus. The forward-trajectory method seeks to answer this question directly.

The way we construct forward trajectories does not collect a complete sample of the in situ cirrus since we consider only those trajectories that start from convec-

tion and last no more than 5 days. In situ cirrus that are beyond the influence of convection more than 5 days are not counted. But we have a complete sample of detrainment cirrus and we can derive a ratio of detrainment cirrus to all cirrus; the remainder is interpreted to be the in situ cirrus. Based on 2 months of global data (January and July of 1996), our estimates of the detrainment cirrus and in situ cirrus fractions of all cirrus (which cover about 0.20 of the whole Tropics from 30°S to 30°N) are about 44% and 56%, respectively. These results agree qualitatively with those of Heymsfield and Donner (1990) in that it indicates that more than half of the tropical cirrus are not produced by convective detrainment but form in situ separately. The probable reason for a quantitative difference in the percentages is that the decaying stages of detrainment cirrus, which have traveled over 600–1000 km from the convection, are counted as in situ cirrus by Heymsfield and Donner (1990). Figure 10 shows the monthly mean distribution of cloud amount for detrainment cirrus and in situ cirrus derived from the analysis described above. Compared to Fig. 2, almost all detrainment cirrus are concentrated in the convective regions and nearby, which is to be expected as they are derived from convection and their lifetime is about 1 day (i.e., the advection distance is less than 1000 km). In situ cirrus, on the other hand, are spread out from the outskirts of the convective regions to the rest of the Tropics.

Pfister et al. (2001) studied thin cirrus near the tropical tropopause (a cirrus type that is not addressed by our study) using aircraft observations coupled with a back-trajectory method; they found two basic types of cirrus: thin quasi-laminar wisps and thick, more textured structures, which are associated with an in situ formation mechanism and nearby convective blowoff, respectively. Massie et al. (2002) used a similar back-trajectory method but applied it to observations from the Halogen Occultation Experiment (HALOE) on the *Upper Atmosphere Research Satellite* (*UARS*). In their study, deep convection was encountered 49% of the time along the 5-day back trajectories for 950 cirrus observations and for the regions from 20°S to 20°N, and from 60°E to 180°. It is noteworthy to point out that cirrus in our study are thicker and lower than the tropical tropopause cirrus (often subvisible), yet a very similar partitioning of detrainment and in situ formation mechanisms is obtained.

6. The relationship between tropical cirrus and upper-tropospheric water vapor

Simply from the understanding of basic cloud physics, we would expect that cirrus and UTWV should track each other since, after all, it is the saturation of water vapor that makes clouds. Although our understanding of ice clouds like cirrus is still rather preliminary, this basic relationship between cirrus and UTWV should still hold in general. The correlation of the maps of cirrus

and UTWV as shown in Fig. 2 and Fig. 4 confirms this relationship. However, a deeper and more detailed understanding of the relationship between cirrus and UTH and how they interact with each requires more careful study beyond the correlation between monthly mean maps. In this section, we examine the relationship and interaction along trajectories between cirrus and UTWV, that is, how cirrus may affect UTWV and vice versa.

As mentioned in section 2, the advantage of using microwave measurements to retrieve UTWV is that they are insensitive to upper-tropospheric, nonprecipitating clouds such as cirrus, thus minimizing the cloud contamination problem and permitting a better sampling of UTWV within cirrus-covered regions. Following the approach of Salathe and Hartmann (1997), we composite many trajectories along each forward air trajectory. Figure 11 shows the composite UTWV as a function of time the air has traveled from convective regions for all trajectories. Forward air trajectories are sorted according to the geographical location of the convective sources: east Indian Ocean and tropical west Pacific, Africa and west Indian Ocean, and South American Amazon. The East Indian Ocean and tropical west Pacific region is moister than the other two regions. For all three regions, UTWV decreases as air makes its way from convective regions to the subtropical dry regions: UTH drops from >60% (close to 100% relative to ice) on the edge of convective regions to about 25%–35% after air has traveled along forward air trajectories for 5 days (i.e., isolated from convection for 5 days).[7] Note from Fig. 4 that this UTH range corresponds to the regions from the edges of the convective systems to the outskirts of the tropical and subtropical dry regions. Figure 11 is consistent with the findings by Salathe and Hartmann (1997) and Soden (1998) concerning how radiatively driven subsidence dries out the tropical upper troposphere outside of the tropical convective regions, except that their studies were confined to the east Pacific; our results confirm that the same pattern holds for the whole Tropics and subtropics. Notably the rate of drying seems uniform over the whole Tropics.

To see how cirrus interact with the UTWV, we consider the composite evolution of UTWV along forward air trajectories based on clear and cloudy cases separately (Fig. 12). Figure 12 shows that UTWV decreases at a much slower rate when cirrus are present: the *e*-folding time for subsidence to dry out the upper troposphere is about 5 days with clear skies (we assume that radiatively driven subsidence is the only process that dries the upper troposphere when there are no upper tropospheric clouds), while it is about 14–15 days for a composite trajectory with cirrus (cirrus amount > 0.80). Soden (1998) showed some similar results by tracking satellite images taken from IR radiances at 6.7 μm, but these

---

[7] UTH is calculated with respect to liquid water. For the temperature range in the upper troposphere, a relative humidity of 70% with respect to liquid water is close to 100% with respect to ice.

Detrainment Cirrus, 9601

In Situ Cirrus, 9601

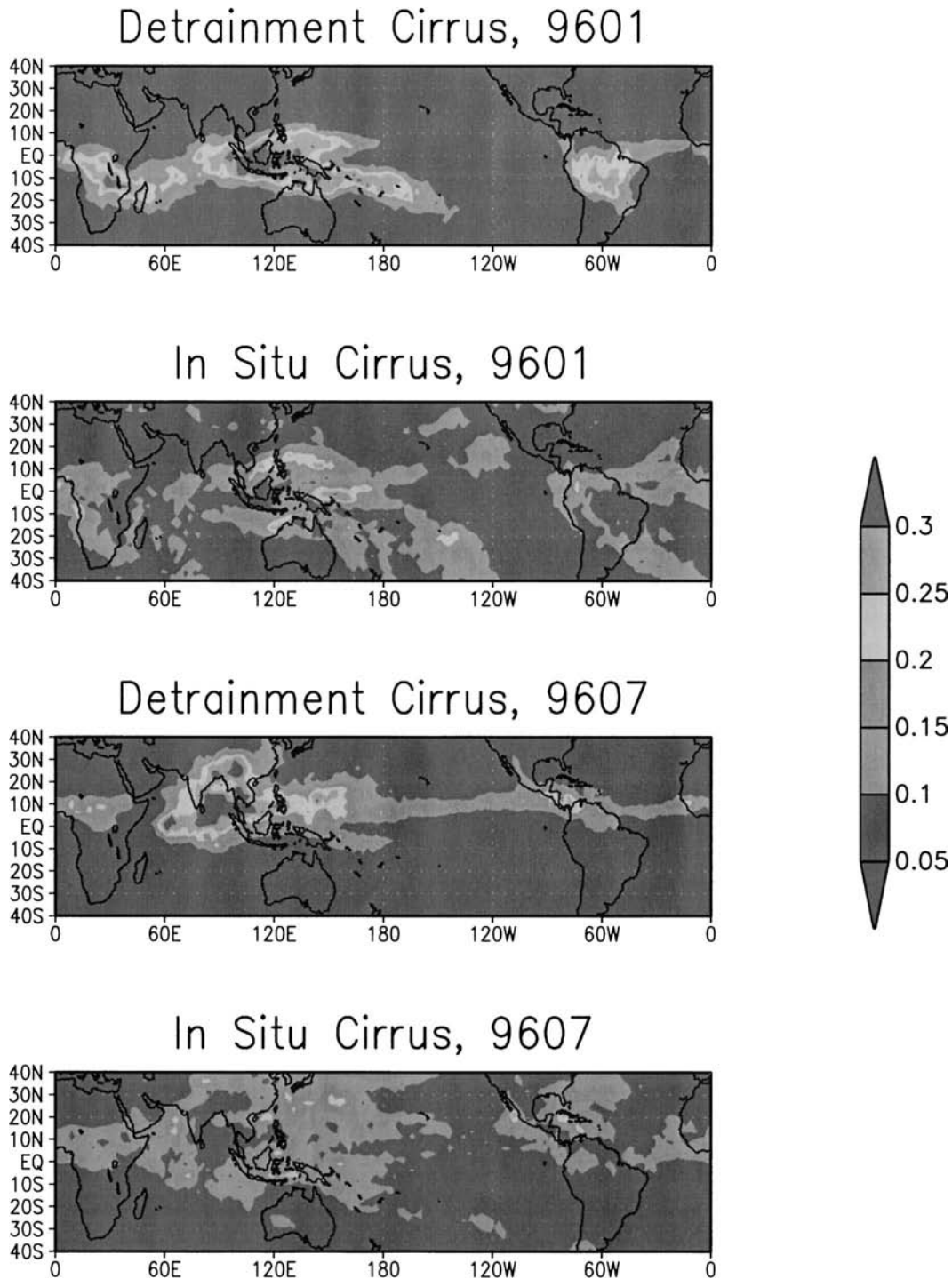## Detrainment Cirrus, 9607

In Situ Cirrus, 9607

FIG. 10. Monthly mean distribution of cloud amount for detrainment cirrus and in situ cirrus.

results might be contaminated by thin cirrus; the fact that both results are qualitatively similar suggests that the "moister" air parcels are more extensive than the associated cirrus as we will show. The regional variations in the rate of decrease of UTWV are much smaller for clear cases than for cirrus cases. Figure 12 suggests that, compared to clear cases, cirrus-covered regions are associated with a moister upper troposphere (instantaneous relation) and a slower rate of UTWV decrease (derivative relation). The former relation is easily derived from comparing Fig. 2 and Fig. 4; the latter relation is the result of the trajectory analysis. One objective of this section is to find
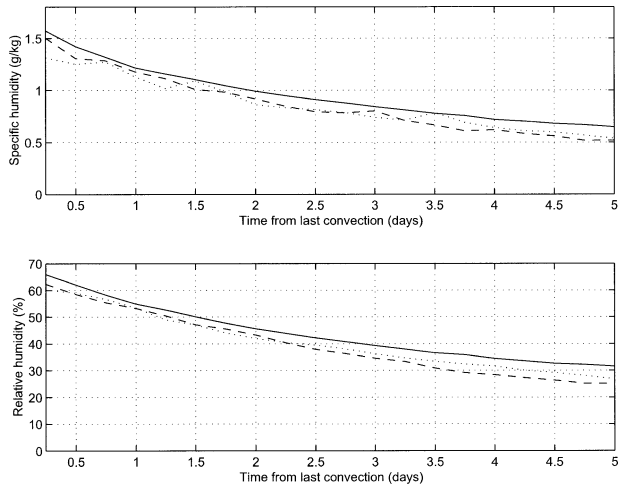
FIG. 11. Composite UTWV along forward trajectories. (top) UTWV as specific humidity (g kg^{-1}) and (bottom) UTWV as relative humidity (%). Three curves in each panel represent the three regions in Fig. 8: the Indian Ocean and west Pacific warm pool (solid), tropical Africa (dashed), and the Amazon and Atlantic (dotted).

out what processes might be responsible for these differences and what role cirrus play in affecting the distribution of UTWV.

Consider UTWV distributions for three categories of clear cases along forward air trajectories: one that has some upstream cirrus history (cirrus amount > 0.30) in the past 12 h (we call it a cirrus-to-clear case), one that has cirrus downstream (clear to cirrus), and one that has been clear for the past or next 12 h (clear-to-clear case). Since we focus on clear scenes only, the comparison has a common reference point (note that this is different from comparing UTWV for clear scenes with UTWV for cloudy scenes since we know that higher values in UTWV are associated with cloudy scenes than with clear scenes). These cases are also sorted out by the time air has traveled from convection because UTWV is a strong function of time from the last convection due to the continuous drying by subsidence (see Figs. 11 and 12). We compare in Fig. 13 the UTH histograms for the cirrus-to-clear, clear-to-cirrus, and clear-to-clear cases for four composite days (days 2–5). UTH in day 1 is not included because moisture within the vicinity of convective regions is close to saturation throughout the whole troposphere and also because clear scenes are rarely seen there. Figure 13 shows that more moisture
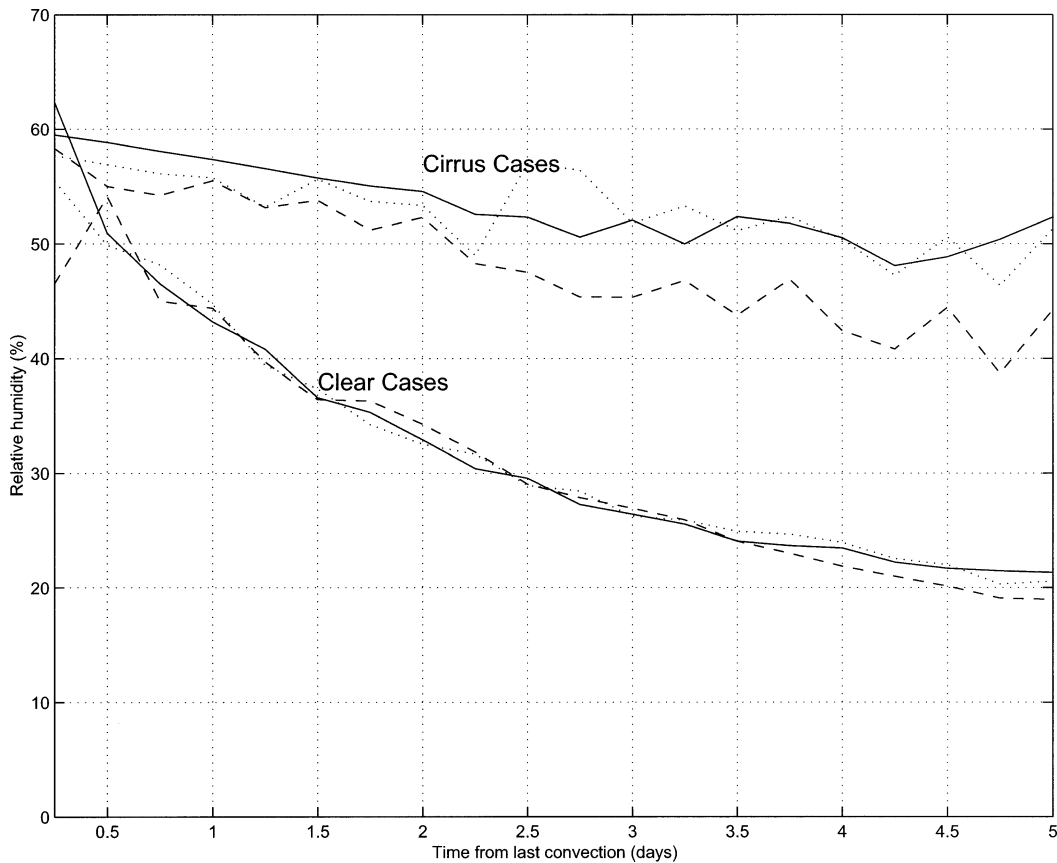

FIG. 12. Composite UTWV (relative humidity) along forward trajectories. Clear and cirrus cases are composited separately. The solid, dashed, and dotted curves represent the same regional variations as in Fig. 11.
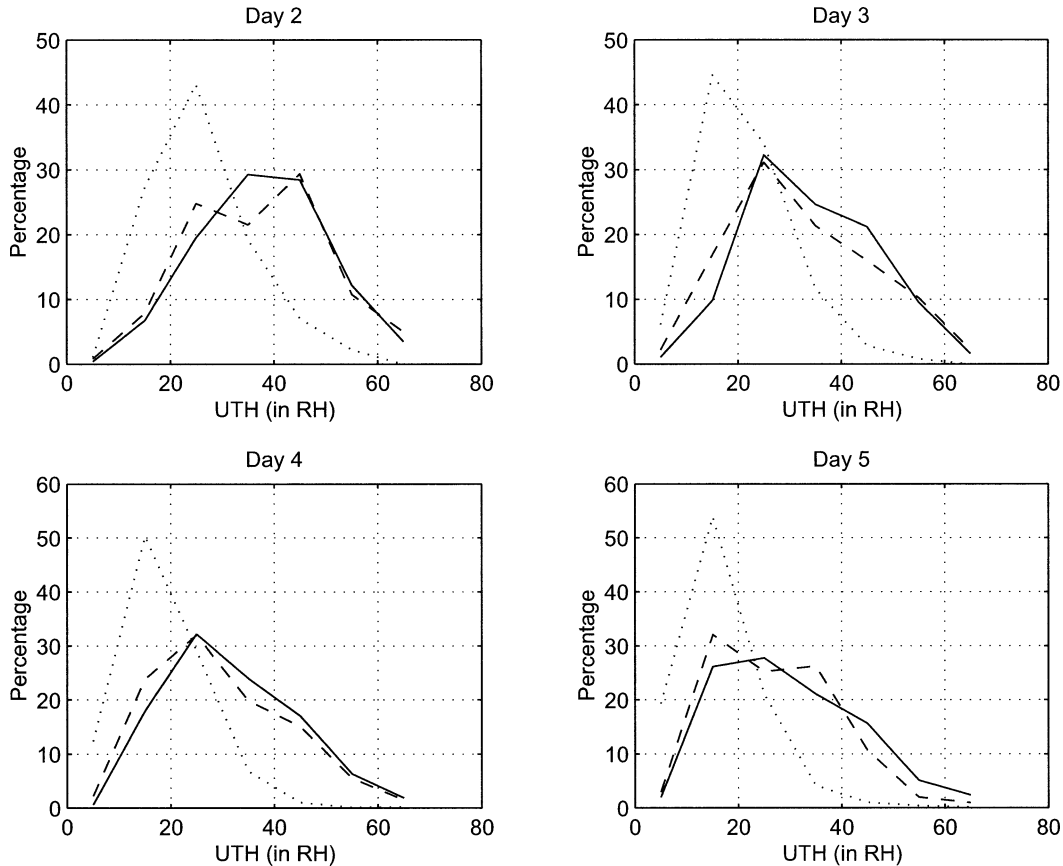
FIG. 13. Histograms of UTH for days 2, 3, 4, and 5 for three categories of clear cases: one that has upstream cirrus history in the past 12 h (solid), one that has cirrus downstream in the next 12 h (dashed), and another that has been clear for the past or future 12 h (dotted).

is contained in the clear upper troposphere with either some upstream or downstream cirrus within 12 h than in previously or subsequently clear situations. Figure 13 goes one step further than Fig. 12 to show that the association between cirrus and a moister upper troposphere is not just instantaneous, but also lasts for some time (at least 12 h): air that produces cirrus later or in which cirrus dissipate is systematically moister than air that is persistently clear.

Figures 13 suggests that the elevated UTWV level has a longer duration than the cirrus. That is, before cirrus form, the upper troposphere is already moister; after cirrus dissipate, the upper troposphere continues to be moister. This indicates that cirrus cannot be responsible for the moister upper troposphere. Two additional results support this conclusion. First, we examine whether water content in cirrus is enough to explain the upper-tropospheric moistening: we compare in Fig. 14 the extra UTWV when cirrus are present (i.e., the difference between the two curves in Fig. 12) with the ice water path (IWP) of cirrus and cirrostratus from Fig. 7. We convert the relative humidity to precipitable water (PW) within a layer of 200–500 mb to facilitate

the comparison with cirrus IWP.[8] Figure 14 shows that the additional moisture in the upper troposphere when cirrus are present is about 50 times greater than the water contained in the cirrus. Evaporating all the ice in the cirrus will not make much difference in the UTWV. Moreover, if the partial coverage of cirrus is considered (i.e., grid average, instead of in-cloud, IWP is considered), the contribution from the evaporation of cloud ice water is even smaller. Therefore, ice water within cirrus can be ruled out as a significant moisture source for the upper troposphere. Rather, the injection by evaporating detrainment cirrostratus appears as a direct source at the beginning of each trajectory.

Second, we examine the vertical motion that is associated with cirrus and clear scenes. Figure 15 shows the histogram of vertically averaged omega wind (500–

[8] The IWP estimated from our cirrus optical thickness values is very dependent on the assumed cloud particle size. We have used a value of effective radius of 30 μm to obtain the values shown in Fig. 14, so the evaporation of thick cirrostratus may indeed be sufficient to explain the moistening if particle sizes are a few times larger, but the particle size in cirrus would have to be 30–50 times larger to cause the same effect.
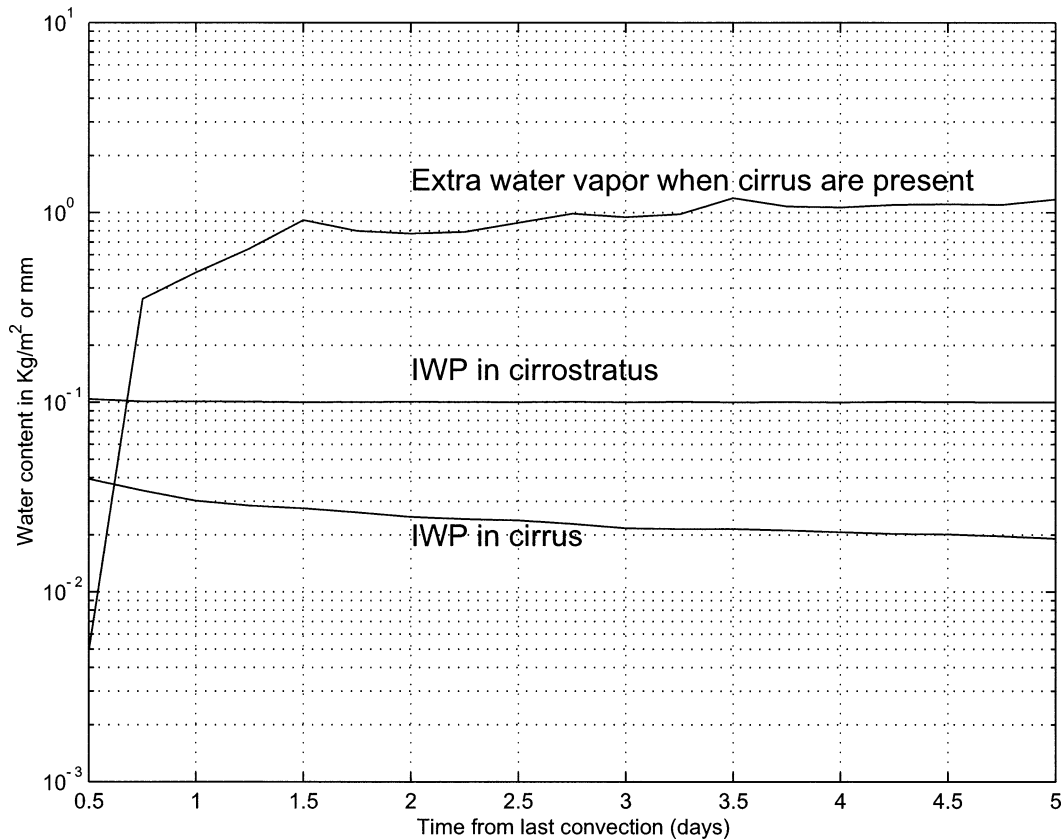
FIG. 14. Comparison between the extra water vapor content in the upper troposphere when cirrus are present and the IWP of cirrus and cirrostratus (see section 2c for the definitions of cirrus and cirrostratus).

200 mb) from the NCEP–NCAR reanalysis for clear and cirrus scenes (cirrus amount > 0.80). Although the instantaneous NCEP–NCAR reanalysis omega wind is considered much less reliable than the horizontal wind, Fig. 15 still shows a tendency for more upward motions to be associated with cirrus occurrence. Interestingly, Fig. 15 also shows that a lot of cirrus occur when there is downward large-scale motion. This may either be due to errors in the NCEP–NCAR reanalysis data or may indicate that subgrid-scale (<2.5° or 280 km) transport of water vapor is producing cirrus within a large-scale subsiding environment.

Therefore, it is likely the transient air motions that moisten the upper troposphere. Transient eddies can transport water vapor upward because of the steep vertical gradient (Del Genio et al. 1994); they can also transport water vapor horizontally (Bates et al. 2001). We argue that these dynamical processes are transporting water vapor vertically because they also form the associated cirrus. Note that this mechanism differs from Sherwood (1999), who proposed a cirrus moistening mechanism that pumps water vapor into the cloudy atmospheric column from surrounding regions by diabatic transports resulting from the local radiative warming effect of cirrus.

7. The maintenance of UTWV along Lagrangian forward trajectories

Previous trajectory studies of UTWV evolution (Salathe and Hartmann 1997; Pierrehumbert and Roca 1998; Dessler and Sherwood 2000) suggested that, compared to subsidence, cirrus play only a minor role in influencing the UTWV because of the small amount of ice water contained in them. Our results confirm this conclusion. However, the presence of cirrus is an indicator of transient upward motions that can also transport moisture upward against the mean subsidence.

There is another way in which cirrus may play an active role in maintaining the UTWV. The sedimentation of ice crystals is an important process that brings condensed water to lower levels (e.g., Rossow 1978). For cirrus formed in situ, the sedimentation process works as a sink for UTWV.[9] In the mature stage of the cirrus life cycle, cloud water removal by sedimentation approximately balances production by condensation

---

[9] Strictly speaking, it is condensation that directly drains the UTWV amount. But sedimentation is the process that moves the condensate away from the upper troposphere, without which it would eventually reevaporate and replace the condensed water vapor.
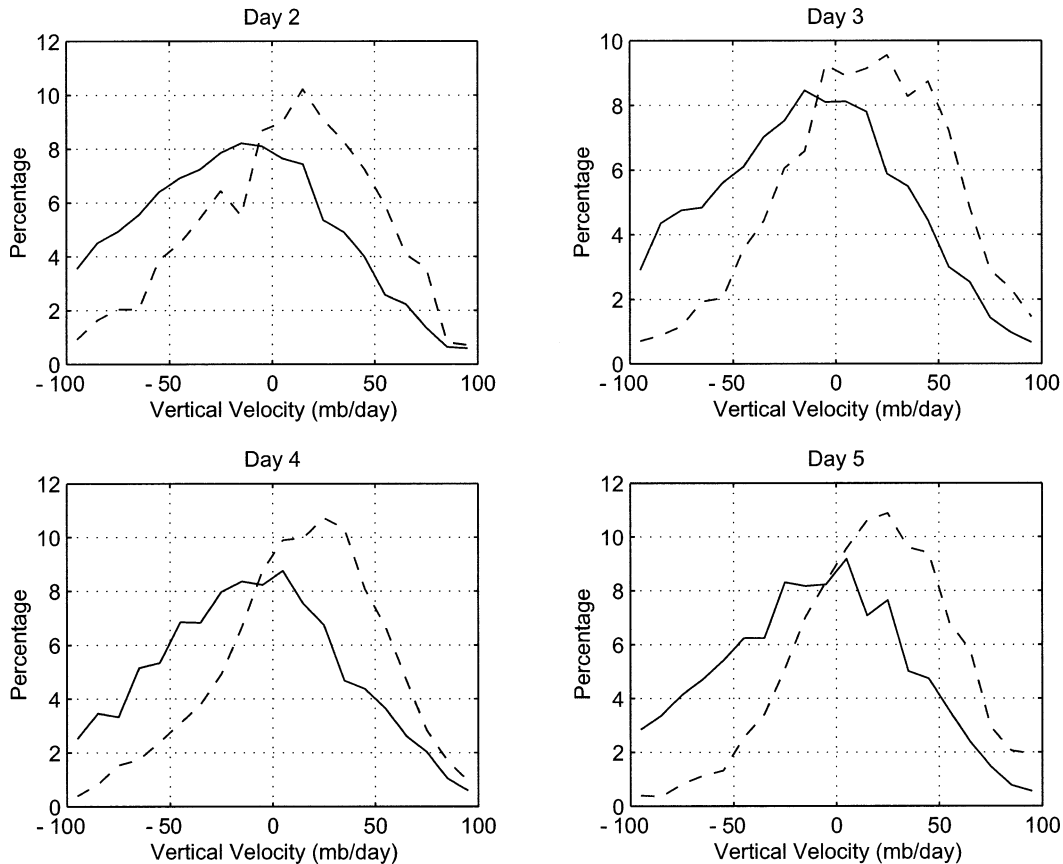
FIG. 15. Histograms of averaged vertical velocity (500–200 mb) for days 2, 3, 4, and 5 from the NCEP–NCAR reanalysis for clear (dashed) and cirrus scenes (solid). Note that negative values correspond to upward motion.

(Heymsfield and Donner 1990). The effectiveness of cirrus as a UTWV sink depends on the ratio of the cirrus lifetime to particle lifetime. Although the cirrus IWC at any moment is small compared to the UTWV amount, cirrus might have a large cloud versus particle lifetime ratio, which could amplify their contribution as a UTWV sink. In other words, if the clouds last much longer than individual ice particles, new particles are replacing those lost by sedimentation, providing a continuous drain of the vapor amount.

We estimate the bracketing values of this vapor sink. The terminal velocity for tropical cirrus particles is about 0.1–1 m s^{-1} for particles ranging from 10 to 100 μm (Heymsfield 2003). The average distance cirrus ice particles fall before leaving the UTWV layer (200–500 mb) is about 3 km. So, the lifetime for ice particles against sedimentation is about 0.8–8 h. Results in section 4c show that the mean lifetime of tropical cirrus is about 19–30 $\pm$ 16 h. So, the removal of water content during a cirrus life cycle is about 3–30 times the ice water contained in the cirrus. The average IWP of tropical cirrus/cirrostratus is about 30 g m^{-2} for in situ cirrus (see Fig. 16). Therefore, during the lifetime of tropical cirrus, the amount of column water removed by the sedimentation process is about 90–900 g m^{-2}, which

might be significant compared to the average UTWV amount (about 3000 g m^{-2}). However, microphysical and dynamic mechanisms governing the role of tropical cirrus as a UTWV sink are still poorly understood. At this time, we are unable to evaluate the importance of this process in a global sense beyond giving these bracketing estimates. Future CloudSat (Stephens et al. 2002) and Cloud–Aerosol Lidar and Infrared Pathfinder Satellite Observations (CALIPSO) cloud profile measurements from space will provide the first global survey of this UTWV sink effect by cirrus particle sedimentation.

Finally, we put together all the information and describe the maintenance of the UTWV along the horizontal trajectories using a simple, conceptual model. The source and sink terms are radiatively driven subsidence and sedimentation of cirrus particles that dry the upper troposphere, while transient transports moisten the upper troposphere supplementing the original injection by convection. Compared to the model used by Salathe and Hartmann (1997), which describes the decrease of UTWV away from convection only as a result of subsidence alone, our model has two more processes (cirrus particle sedimentation and transient transports) that help maintain the UTWV in cloudier regions (cf.
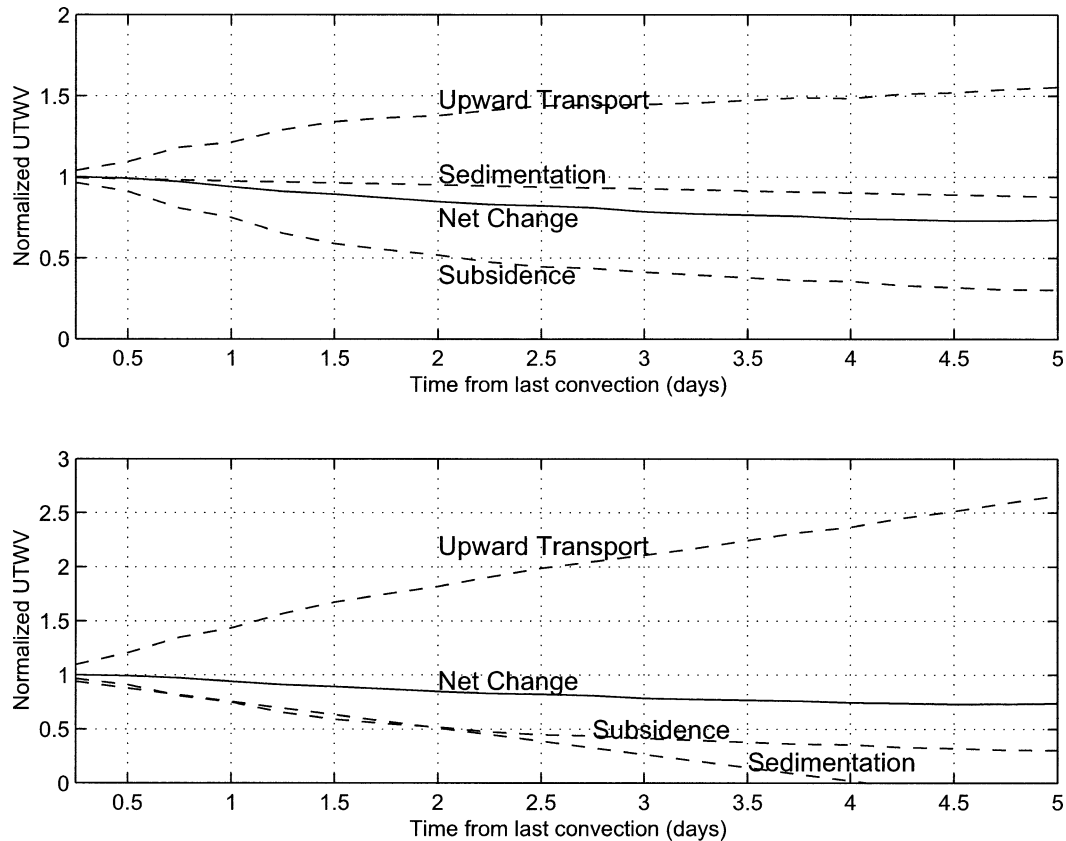
FIG. 16. The normalized evolution of the UTWV along the horizontal trajectories when cirrus occur. Plotted are both the net change (solid curve) and the source/sink terms (dashed curves). (top) Assumes the minimum estimate of the cirrus sedimentation rate, and (bottom) assumes the maximum estimate. See text for details.

Fig. 12). Subsidence is assumed to be the only process that depletes the UTWV in clear regions so its magnitude can be estimated from the clear curve in Fig. 13.[10] The estimate of the cirrus particle sedimentation rate is given in the previous paragraph. The net effect, when the three processes compete with each other to determine the UTWV, is estimated from the curve for cirrus cases in Fig. 12. The transient transport is then calculated as the residual term.

Figure 16 shows the composite evolution of UTWV normalized by the initial value (i.e., the value when the air leaves the convective regions at ice saturation) along the horizontal trajectories when cirrus occur, as well as the corresponding source and sink terms discussed in the conceptual model. There are two versions shown for the two bracketing particle sedimentation rates. The figure shows that when cirrus are present, the maintenance of the UTWV is different from that of the clear case. The significance of the cirrus moisture sink depends on the ice particle sedimentation speed and cirrus lifetime. Cirrus particle sedimentation, together with large-scale

[10] By doing so, we actually assume no other transport for the clear case. This may mean that our estimate of the large-scale subsidence sink is an underestimate.

subsidence, dries out the upper troposphere, while some transport process brings water vapor into the moister regions to counteract the drying processes. The net effect is a much slower drying rate along cloudy horizontal trajectories.

Large-scale subsidence is a process that is continuously at work away from the convective regions (driven by the general radiative cooling of the air). Cirrus microphysics and upward transport of water vapor, on the other hand, are transient processes whose duration depends on factors such as cloud lifetime and wave dynamics. It is unlikely that cirrus and upward transport of water vapor persist for five consecutive days after air leaves convection. Rather, Fig. 16 should be interpreted in terms of net tendencies. For example, Fig. 16 shows that cirrus particle sedimentation, if acting alone, would dry the upper troposphere by 10%–120% (depending on cirrus microphysics) in a 5-day period (this drying would not occur without some motions lifting the air). But the lifetime of cirrus (about 1 day) limits this process to the times when cirrus are present. Hence, the composite picture illustrates the magnitude of each individual source and sink term for the UTWV, which should be considered together with their occurrence fre-

quency and duration to correctly estimate their influence on the evolution of the UTWV.

8. Summary and discussion

The life cycle and evolution of tropical cirrus systems and their relation to the upper-tropospheric water vapor (UTWV) are examined by analyzing satellite-derived cloud data, UTWV data, and NCEP–NCAR reanalysis wind field data in a Lagrangian framework. In this section, we summarize our results and examine their implications for cirrus modeling and for cirrus–UTWV feedback on climate changes.

The Lagrangian trajectory analysis shows that the decay of deep convection is followed by the growth of cirrostratus and cirrus and then the decay of cirrostratus is followed by the continued growth of cirrus. Cirrus properties continue to evolve along their trajectories as they gradually thin out and move to the lower levels. These detrainment cirrus systems last for 19 ± 16 h. An estimate of cirrus particle lifetimes, however, gives a range from 0.8 to 8 h, depending on particle terminal velocity (Heymsfield 2003). The difference suggests that there are at least transient upward motions that oppose particle sedimentation to maintain tropical cirrus and to keep them from dissipating for much longer than the particle lifetime. Consequently, cirrus can advect over large distances, about 600–1000 km, during their lifetimes. For almost all current GCMs, this distance spans many grid boxes requiring that the water vapor and cloud water budgets include an advection term. All these results concerning cirrus evolution and life cycle variation provide the observational basis for improving and validating cirrus modeling in GCMs. Comparison of the geographical patterns of cirrus between a model and observations is not a very informative test of the model because it cannot distinguish between the causes for disagreements, which might involve other factors, such as the model treatment of deep convective anvils and the large-scale circulation (cf. Salathe and Hartmann 2000). Comparison of cirrus evolution and life cycle in a Lagrangian framework, on the other hand, provides a way of focusing on the formation–decay processes that control the cirrus properties.

Detrainment cirrus are distinguished from in situ cirrus in this study. Our results show that more than half of the tropical cirrus (56%) are produced in situ well away from any significant convection. The different generating mechanisms for these two types of cirrus suggest the possibility that they may not respond in the same way to a changing climate, producing different feedbacks. Detrainment cirrus have a strong connection to deep convection, being produced as the decay products of the convective anvil clouds. A change of this type of cirrus with climate should be understood as part of the study of how convection changes with climate. But in situ cirrus, which we find to be an equally abundant type, are not directly connected with convection

(convection may act as one source of water vapor for their formation, although the study shows that the air leaving the vicinity of convective systems monotonically dries out). In situ cirrus can be produced by other dynamical processes, such as small-scale turbulent motions, gravity waves, large-scale waves or episodes of large-scale uplift; their response to a changing climate therefore depends on how these other dynamic processes change.

Chou and Neelin (1999) studied the relationship between cirrus coverage and convective cloud-top temperature and found that deep convection with colder cloud tops produces more cirrus [cf. Machado and Rossow (1993), who show that colder tops are associated with larger convective systems with more water in their associated stratiform clouds]. Taken together with the assumption that convective cloud-top temperature decreases with increasing surface temperature, these relationships imply a positive cirrus feedback on temperature. Lindzen et al. (2001), on the other hand, proposed a negative cirrus feedback as they found that cirrus coverage decreases with increasing SST when averaged over a large region. Some of the differences in such findings may arise from analysis in different parts of the Tropics, which have more or less convective detrainment cirrus. Overall, our results show that only about half of tropical cirrus are directly related to convection. The finding that tropical cirrus are of two distinct types, possibly with different responses to climate change, makes the problem of determining cirrus-climate feedback much more complicated than previously thought, including the possibility that the overall feedback is different in different portions of the Tropics.

The interaction between cirrus and UTWV is explored by comparing the evolution of the UTWV along composite clear trajectories and trajectories with cirrus. Microwave radiance measurements make it possible to sample cirrus and UTWV simultaneously, thus eliminating possible clear-sky biases associated with the use of IR radiances confined to cloud-free regions. Our results show that cirrus are associated with a moister upper troposphere and that UTWV decreases more slowly with time when cirrus are present. Careful examination of the data also indicates that the elevated UTWV level has a longer duration than the cirrus. That is, before cirrus form, the upper troposphere is already moister; after cirrus dissipate, the upper troposphere continues to be moister, which suggests that tropical cirrus are probably the result, rather than the cause, of the moist upper troposphere. This association makes sense if the same transient motions are responsible for both vertical vapor transport and cloud formation. The amount of water in cirrus is much too small for the evaporation of cirrus ice particles to moisten the upper troposphere significantly, but cycling of vapor into cloud particles that fall could mean that cirrus sedimentation might be a significant vapor sink if the particles grow large enough. The vertical velocities in the NCEP–NCAR re-

analysis, even though they may be unreliable, still show a tendency for cirrus to be associated more with updrafts compared to clear sky, although a lot of the time the large-scale mean vertical motion is still downward. This also suggests a role for transient motions that transport water vapor and produce the cirrus.

Finally, we discuss the evolution and maintenance of the UTWV along forward trajectories by using a simple, conceptual model, which considers three processes that compete with each other to determine UTWV: large-scale mean subsidence, cirrus ice particle sedimentation, and upward transport by transient motions. The former two are sinks and the latter a source. The sink caused by cirrus ice crystal sedimentation may not be negligible because of the large cloud versus particle lifetime ratio. To correctly simulate UTWV feedback in a changing climate, models need to have a detailed treatment of cirrus microphysics.

REFERENCES

Bates, J. J., D. L. Jackson, F-M. Breon, and Z. D. Bergen, 2001: Variability of tropical upper tropospheric humidity 1989–1998. *J. Geophys. Res.,* **106,** 32 271–32 281.

Berg, W., J. J. Bates, and D. L. Jackson, 1999: Analysis of upper-tropospheric water vapor brightness temperature from SSM/T2, HIRS, and GMS-5 VISSR. *J. Appl. Meteor.,* **38,** 580–595.

Bretherton, C. S., and R. Pincus, 1995: Cloudiness and marine boundary layer dynamics in the ASTEX Lagrangian experiments. Part I: Synoptic setting and vertical structure. *J. Atmos. Sci.,* **52,** 2707–2723.

Chahine, M. T., 1974: Remote sounding of cloudy atmospheres. I: The single cloud layer. *J. Atmos. Sci.,* **31,** 233–243.

Chou, C., and J. D. Neelin, 1999: Cirrus detrainment-temperature feedback. *Geophys. Res. Lett.,* **26,** 1295–1298.

Cooper, S. J., T. S. L'Ecuyer, and G. L. Stephens, 2003: The impact of explicit cloud boundary information on ice cloud microphysical property retrievals from infrared radiances. *J. Geophys. Res.,* **108,** 4107, doi:10.1029/2002JD002611.

Del Genio, A. D., W. J. Kovari, and M.-S. Yao, 1994: Climatic implications of the seasonal variation of upper tropospheric water vapor. *Geophys. Res. Lett.,* **21,** 2701–2704.

Dessler, A. E., and S. C. Sherwood, 2000: Simulation of tropical upper tropospheric humidity. *J. Geophy. Res.,* **105,** 20 155–20 163.

Engelen, R. J., and G. L. Stephens, 1998: Comparison between TOVS/HIRS and SSM/T2-derived upper-tropospheric humidity. *Bull. Amer. Meteor. Soc.,* **79,** 2748–2751.

Falcone, V. J., and Coauthors, 1992: DMSP F11 SSM/T-2 calibration and validation data analysis. Environmental Research Paper IIII, Phillips Laboratory Tech. Rep., 108 pp.

Giraud, V., J. C. Buriez, Y. Fouquart, and F. Parol, 1997: Large-scale analysis of cirrus clouds from AVHRR data: Assessment of both a microphysical index and cloud-top temperature. *J. Appl. Meteor.,* **36,** 664–675.

Greenwald, T. J., and S. A. Christopher, 2002: Effect of cold clouds on satellite measurements near 183 GHz. *J. Geophys. Res.,* **107,** 4170, doi:10.1029/2000JD000258.

Heymsfield, A. J., 2003: Properties of tropical and midlatitude ice cloud particle ensembles: Part I: Median mass diameters and terminal velocities. *J. Atmos. Sci.,* **60,** 2573–2591.

——, and L. J. Donner, 1990: A scheme for parameterizing ice-cloud content in general circulation models. *J. Atmos. Sci.,* **47,** 1865–1877.

——, and G. M. McFarquhar, 1996: High albedos of cirrus in the tropical Pacific warm pool: Microphysical interpretations from CEPEX and from Kwajalein, Marshall Islands. *J. Atmos. Sci.,* **53,** 2424–2451.

Inoue, T., 1985: On the temperature and effect emissivity determination of semitransparent cirrus clouds by bispectral measurements in the 10 μm window region. *J. Meteor. Soc. Japan,* **63,** 88–98.

Jensen, E., L. Pfister, A. S. Ackerman, A. Tabazadeh, and O. B. Toon, 2001a: A conceptual model of the dehydration of air due to freeze-drying by optically thin, laminar cirrus rising slowly across the tropical tropopause. *J. Geophys. Res.,* **106** (D15), 17 237–17 252.

——, and Coauthors, 2001b: Prevalence of ice-supersaturated regions in the upper troposphere: Implication for optically thin ice cloud formation. *J. Geophys. Res.,* **106** (D15), 17 253–17 266.

Jin, Y., 1998: Investigation of cirrus by satellite remote sensing. Ph.D. dissertation, Columbia University, 104 pp.

——, and W. B. Rossow, 1997: Detection of cirrus overlapping low-level clouds. *J. Geophys. Res.,* **102,** 1727–1737.

——, ——, and D. P. Wylie, 1996: Comparison of the climatologies of high-level clouds from HIRS and ISCCP. *J. Climate,* **9,** 2850–2879.

Kalnay, E., and Coauthors, 1996: The NCEP/NCAR 40-Year Reanalysis Project. *Bull. Amer. Meteor. Soc.,* **77,** 437–471.

Key, J., 1996: Streamer user's guide. Dept. of Geography Tech. Rep. 96-01, Boston University, Boston, MA, 91 pp.

Kidder, S. Q., and T. H. Vonder Haar, 1995: *Satellite Meteorology: An Introduction.* Academic Press, 466 pp.

Liao, X., W. B. Rossow, and D. Rind, 1995a: Comparison between SAGE II and ISCCP high-level clouds. Part 1: Global and zonal mean cloud amounts. *J. Geophys. Res.,* **100,** 1121–1135.

——, ——, and ——, 1956b: Comparison between SAGE II and ISCCP high-level clouds. Part 2: Locating cloud tops. *J. Geophys. Res.,* **100,** 1137–1147.

Lindzen, R. S., M. D. Chou, and A. Y. Hou, 2001: Does the earth have an adaptive infrared iris? *Bull. Amer. Meteor. Soc.,* **32,** 417–432.

Liou, K. N., S. C. Ou, Y. Takano, F. P. J. Valero, and T. P. Ackerman, 1990: Remote sounding of the tropical cirrus cloud temperature and optical depth using 6.5 and 10.5 μm radiometers during STEP. *J. Appl. Meteor.,* **29,** 716–726.

Luo, Z., 2003: Investigation of tropical cirrus, their variability, evolution, and relation to the upper tropospheric water vapor. Ph.D. dissertation, Columbia University, 148 pp.

——, W. B. Rossow, T. Inoue, and C. J. Stubenrauch, 2002: Did the eruption of the Mt. Pinatubo volcano affect cirrus properties? *J. Climate,* **15,** 2806–2820.

Machado, L. A. T., and W. B. Rossow, 1993: Structural characteristics and radiative properties of tropical cloud clusters. *Mon. Wea. Rev.,* **121,** 3234–3260.

——, ——, R. L. Guedes, and A. W. Walker, 1998: Life cycle variations of mesoscale convective systems over Americas. *Mon. Wea. Rev.,* **125,** 1630–1654.

Massie, S., A. Gettelman, and W. Randel, 2002: Distribution of tropical cirrus in relation to convection. *J. Geophys. Res.,* **107,** 4591, doi:10.1029/2001JD001293.

McFarquhar, G. M., and A. J. Heymsfield, 1996: Microphysical char-

acteristics of three anvils sampled during the Central Equatorial Pacific Experiment. *J. Atmos. Sci.,* **53,** 2401–2423.

Moody, J. L., A. J. Wimmers, and J. C. Davenport, 1999: Remote sensed specific humidity: Development of a derived product from the GOES Imager Channel 3. *Geophys. Res. Lett.,* **26,** 59–62.

Parol, F., J. C. Buriez, G. Brogniez, and Y. Fouquart, 1991: Information content of AVHRR channel 4 and 5 with respect to the effective radius of cirrus cloud particles. *J. Appl. Meteor.,* **30,** 973–984.

Pfister, L., and Coauthors, 2001: Aircraft observations of thin cirrus clouds near the tropical tropopause. *J. Geophys. Res.,* **106,** 9765–9786.

Pierrehumbert, R. T., and R. Roca, 1998: Evidence for control of Atlantic subtropical humidity by large scale advection. *Geophys. Res. Lett.,* **25,** 4537–4540.

Pincus, R., M. B. Baker, and C. S. Bretherton, 1997: What controls stratocumulus radiative properties? Lagrangian observations of cloud evolution. *J. Atmos. Sci.,* **54,** 2215–2236.

Prabhakara, C., R. S. Fraser, G. Dalu, M.-L. Wu, and R. J. Curran, 1988: Thin cirrus clouds: Seasonal distribution over oceans from Nimbus-4 IRIS. *J. Appl. Meteor.,* **27,** 379–399.

Ramanathan, V., and W. Collins, 1991: Thermodynamic regulation of ocean warming by cirrus clouds deduced from observations of the 1987 El Niño. *Nature,* **351,** 27–32.

Rossow, W. B., 1978: Cloud microphysics: Analysis of the clouds of Earth, Venus, Mars, and Jupiter. *Icarus,* **36,** 1–50.

——, and R. A. Schiffer, 1991: ISCCP cloud data products. *Bull. Amer. Meteor. Soc.,* **72,** 2–20.

——, and ——, 1999: Advances in understanding clouds from ISCCP. *Bull. Amer. Meteor. Soc.,* **80,** 2261–2287.

——, W. Walker, D. Beuschel, and M. Roiter, 1996: International Satellite Cloud Climatology Project (ISCCP) documentation of new datasets. WMO TECH. DOC. 737, World Climate Research Programme.

Salathe, E. P., and D. L. Hartmann, 1997: A trajectory analysis of tropical upper-tropospheric moisture and convection. *J. Climate,* **10,** 2533–2547.

——, and ——, 2000: Subsidence and upper-tropospheric drying along trajectories in a general circulation model. *J. Climate,* **13,** 257–263.

Schiffer, R. A., and W. B. Rossow, 1983: The International Satellite Cloud Climatology Project (ISCCP): The first project of the World Climate Research Programme. *Bull. Amer. Meteor. Soc.,* **64,** 779–784.

Sherwood, S. C., 1999: On moistening of the tropical troposphere by cirrus clouds. *J. Geophys. Res.,* **104,** 11 949–11 960.

Soden, B. J., 1998: Tracking upper tropospheric water vapor radiances: A satellite perspective. *J. Geophys. Res.,* **103,** 17 069–17 081.

——, and F. P. Bretherton, 1993: Upper tropospheric relative humidity from the GOES 6.7 μm channel: Method and climatology for July 1987. *J. Geophys. Res.,* **98,** 16 669–16 688.

Stephens, G. L., and Coauthors, 2002: The CloudSat mission and the A-Train: A new dimension of space-based observations of clouds and precipitation. *Bull. Amer. Meteor. Soc.,* **83,** 1771–1790.

Stubenrauch, C. J., A. Chedin, R. Armante, and N. A. Scott, 1999a: Clouds as seen by satellite sounders (3I) and imagers (ISCCP). Part II: A new approach for cloud parameter determination in the 3I algorithm. *J. Climate,* **12,** 2214–2223.

——, W. B. Rossow, F. Cheruy, A. Chedin, and N. A. Scott, 1999b: Clouds as seen by satellite sounders (3I) and imagers (ISCCP). Part I: Evaluation of cloud parameters. *J. Climate,* **12,** 2189–2213.

Sun, D.-Z., and R. S. Lindzen, 1993: Distribution of tropical tropospheric water vapor. *J. Atmos. Sci.,* **50,** 1643–1660.

Szejwach, G., 1982: Determination of semi-transparent cirrus cloud temperature from infrared radiances: Application to METEO-SAT. *J. Appl. Meteor.,* **21,** 384–393.

Wang, P., P. Minnis, M. P. McCormick, G. S. Kent, and K. M. Skeens, 1996: A 6-year climatology of cloud occurrence frequency from Stratospheric Aerosol and Gas Experiment II observations (1985–1990). *J. Geophys. Res.,* **101,** 29 407–29 429.

Wu, M. C., 1987: A method for remote sensing the emissivity, fractional cloud cover, and cloud top temperature of high-level, thin clouds. *J. Climate Appl. Meteor.,* **26,** 225–233.

Wylie, D. P., and W. P. Menzel, 1999: Eight years of high cloud statistics using HIRS. *J. Climate,* **12,** 170–184.

——, ——, H. M. Woolf, and K. I. Strabala, 1994: Four years of global cirrus cloud statistics using HIRS. *J. Climate,* **7,** 1972–1986.

Ye, B., 2000: Cumulus anvil cloud properties, large-scale condition, and climate change. Ph.D. dissertation, Columbia University, 220 pp.